CHALMERS
UNIVERSITY OF TECHNOLOGY

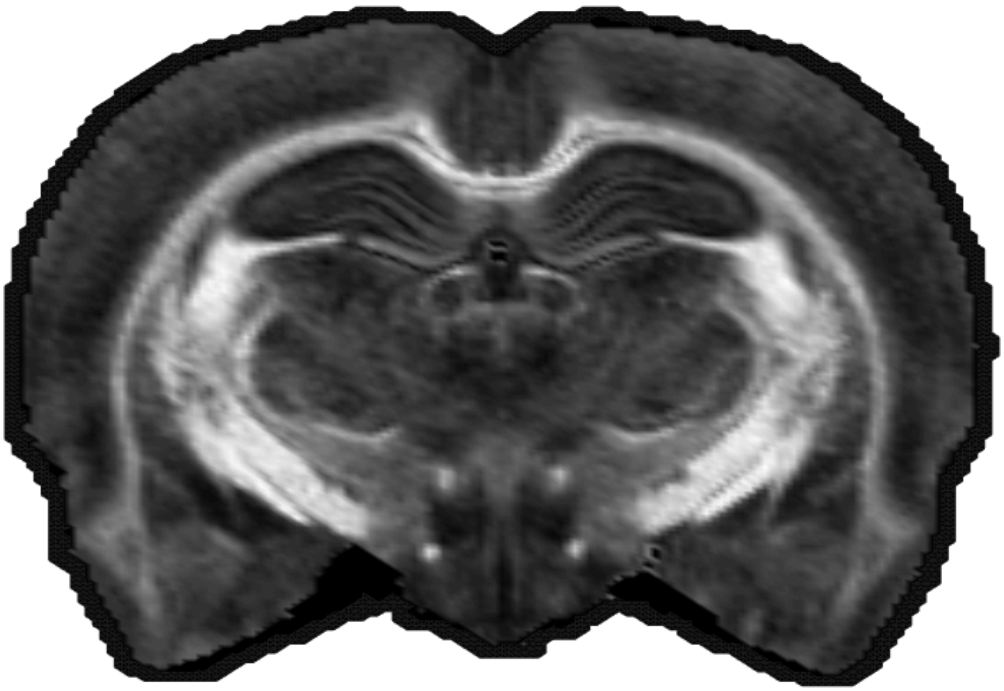

Developing a Protocol for Detection of Axonal Injury in Rats Using Diffusion Tensor Magnetic Resonance Imaging

Evaluating large volumes of data to find microscopic injuries

Master's thesis in Biomedical Engineering

HANNA KVISTBERG AND MARTIN LUNDGREN

Department of Applied Mechanics
CHALMERS UNIVERSITY OF TECHNOLOGY
Gothenburg, Sweden 2015

Master's thesis 2015:27

Developing a Protocol for Detection of Axonal Injury in Rats Using Diffusion Tensor Magnetic Resonance Imaging

Evaluating large volumes of data to find microscopic injuries

HANNA KVISTBERG AND MARTIN LUNDGREN

CHALMERS
UNIVERSITY OF TECHNOLOGY

Department of Applied Mechanics
Division of Vehicle Safety
Passive Safety
Chalmers University of Technology
Gothenburg, Sweden 2015

Developing a Protocol for Detection of Axonal Injury in Rats
Using Diffusion Tensor Magnetic Resonance Imaging
Evaluating large volumes of data to find microscopic injuries
HANNA KVISTBERG AND MARTIN LUNDGREN

Supervisor: Johan Davidsson, Department of Applied Mechanics
Examiner: Johan Davidsson, Department of Applied Mechanics

Master's Thesis 2015:27
Department of Applied Mechanics
Division of Vehicle Safety
Passive Safety
Chalmers University of Technology
SE-412 96 Gothenburg
Telephone +46 31 772 1000

Cover: Image of fractional anisotropy values of a slice from an uninjured animal, the one used as target for spatial normalization in section 4.6.

Typeset in LaTeX
Printed by Chalmers Reproservice
Gothenburg, Sweden 2015

Developing a Protocol for Detection of Axonal Injury in Rats
Using Diffusion Tensor Magnetic Resonance Imaging
Evaluating large volumes of data to find microscopic injuries
HANNA KVISTBERG AND MARTIN LUNDGREN
Department of Applied Mechanics
Chalmers University of Technology

Abstract

Traumatic brain injury is a serious injury that is all too common. Commonly traumatic brain injury includes stretching of the axons which is due to the movement of the brain. Today it is not possible to detect axonal injury using conventional imaging techniques, but the possibility to do so would provide superior screenings for injury and guide treatment of patients. The goal of this thesis was to examine the possibility of creating a new protocol for detection of such injuries. Diffusion tensor magnetic resonance images from animal studies on rats, five exposed and four normals, have been studied. The main focus of this thesis was to attempt to differentiate the datasets and find injuries located in the corpus callosum. The study began with examining the results of a previous study carried out on the same dataset. This examination was followed by evaluating fractional anisotropy and tractography, with the conclusion that fractional anisotropy can be useful but possibly insufficient for detection of axonal injuries when the spatial resolution is too high. Since fractional anisotropy stays the same in points where all eigenvalues increase or decreases equally, injuries might go undetected. Tractography suffers from a few problems underlying with DT-MRI itself, namely the poor ability to resolve crossing fibers, but can be a useful tool in smaller brain regions. Further attempts at spatial normalization and amplitude normalization was made to facilitate a voxel-wise analysis of the brain, comparing each voxel of the traumatized and aligned brains with the voxels of healthy animals. The results did not show significant differences between the healthy and injured animals. Attempts at using classifiers to differentiate between the animals were made, using both neural networks and a linear discriminant analysis classifier. For the neural network classifier this seems promising, but the number of animals in the study was not large enough to be able to perform a complete evaluation. Suggestions on how to improve detection of axonal injuries and verifying the possibility to do so are presented; such as using phantoms to be able to place controlled injuries simulating axonal injuries and comparing images before and after introducing the injury. Such an approach would facilitate detection of diffuse axonal injury by ensuring that a detected difference stems from the injury alone.

Keywords: DT-MRI, Axonal Injury, Classification, Normalization, Spatial Normalization, Traumatic Brain Injury, Tractography, Corpus Callosum and Fractional Anisotropy.

Acknowledgements

We would like to thank our supervisor and examiner Johan Davidsson, Associate professor, Applied mechanics for guidance and assistance, as well as sharing unpublished results with us.
We would also like to thank Marta Carcedo for her earlier work on this topic, which has been useful when getting to know the subjects and the topic.
We would also like to thank Peter Damberg, Mårten Risling, Stefan Plantman and Anders Hånell from Karolinska institutet, for providing scientific guidance and expertise for this thesis.
Our opponent Jonathan Jonsson has provided us with useful feedback and comments which have helped improve the report considerably.
Finally, we would like to thank our friends and family for support and proofreading.

Hanna Kvistberg and Martin Lundgren, Gothenburg, June 2015

Contents

List of Figures

List of Tables

1

Introduction

Traumatic brain injury (TBI) is a very common type of injury. It occurs when a blow is delivered to the head or a foreign object penetrates the skull and damages the brain (American Association of Neurological Surgeons, 2011). The injury may occur after a fall, a car crash, a sport accident or being exposed to a blast, which can lead to alteration in the brain function. The symptoms from a TBI varies from case to case but common effects are memory loss, trouble with orientation, in some cases loss of consciousness and in worse cases disability or death (Manley and Maas, 2013). In the United States alone, there were 2.5 million emergency department visits related to TBI in 2010 and TBI contributed to one third of all injury-related deaths (Centers for Disease Control and Prevention, 2015) (Manley and Maas, 2013), and it's been estimated that approximately half of the patients with severe head injury have diffuse axonal injuries (Meythaler et al., 2001), but a more recent study on patients that became disabled after a head trauma found that as many as 58% of the patients had axonal injuries Adams et al. (2011).

Detecting TBIs is important to provide proper diagnosis of the injury, rather than diagnosis based on symptoms. Computer Tomography (CT) is conventionally used because it can distinguish swelling and bleeding in tissue effectively. CT, however, is limited when it comes to detecting Axonal Injuries (AI), also known as nerve fibre injuries, and other current methods such as Magnetic Resonance Imaging (MRI) do not fare any better. Two other common imaging modalities, positron emission tomography and single-photon emission computed tomography are not commonly used in acute situations according to Lee and Newberg (2005), and since they provide functional information rather than anatomical, are unlikely to increase much in usage. Injured axons can cause complications and alteration in the brain tissues that produce symptoms that may be detected several years after the initial injury. A TBI can be a combination of AI, swelling and bleeding. The problem is that detection of bundles of axons is difficult and when the injury is not very large, it typically goes undetected. The human brain's axons vary in size but most are about one to two micrometers in diameter (Komlosh et al., 2013). Therefore, if only a few are injured, they are currently only visible under a microscope. Improved imaging protocols could provide a way to detect these injuries without invasive procedures, which would help diagnosis and improve screening for injury and evaluation of treatments.

1.1 Brain anatomy and injury mechanisms

The brain is one of the largest organs in the human body. It consists mainly of neurons and neuroglia and is divided into four major regions: The brain stem, diencephalon, cerebrum and cerebellum (Tortora and Derrickson, 2013). Larger widespread regions are grouped together as either white matter or gray matter. The cerebrum is divided into two hemispheres. These two hemispheres are connected through the corpus callosum (Seel, 2012), which is a band of white matter, which in turn consists of nervous tissue. The white matter consists primarily of myelinated axons and the gray matter is a combination of neuronal cell bodies, dendrites, unmyelited axons, axon terminals and neuroglia. All these nerve cells are of microscopic size (Tortora and Derrickson, 2013).
The human skull consists of multiple different regions of bones. Those of interest in this thesis are the ones on top of the skull. They are divided into three parts: frontal bone, right- and left parietal bone. They are separated by the coronal suture and the sagittal suture, see figure 1.1. Bregma is the anatomical point on top of the skull where the sagittal- and coronal sutures merge. It is used as a reference point when dividing the brain into slices in the various planes. Such a reference is useful in order to be able to have a fix reference point to compare between subjects when comparing where injuries occur.
When a brain is subjected to trauma a local injury can be caused close to the impact point. The impact may also cause a contrecoup injury (Shaw, 2002). The contrecoup injury is when the brain strikes the interior skull on the opposite side of the impact. Even if the skull is not penetrated or fractured, there might still be damage to the brain, such as bruising and hemorrhage at the position of the impact or the opposite side of the skull. Secondary effects caused by the trauma are pressure change due to swelling of the brain and changes in cerebral blood flow. Both of these effects can be life threatening (Silver et al., 2011). Another consequence of an impact trauma is when nerve cells and supporting cells are stretched due to the movement of the brain causing damage to these cells. Animal models can be an efficient way to study brain injuries (Tortora and Derrickson, 2013), in this study they where useful since they allow for ex-vivo imaging, which reduces major artifacts such as motion, breathing and blood flow.

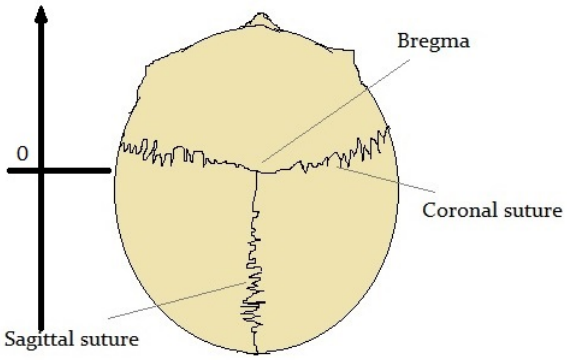

Figure 1.1: A human skull viewed from above to visualize bregma. The top of the image displays front of the skull, and the arrow indicates the direction of the positive offset from bregma, with the zero point indicating no offset from bregma.

1.2 Animal model for injury detection

One of the reasons why animal models are used is to improve the understanding of injuries and to be able to develop treatments. For TBI it's especially useful since the injuries are complex and pathophysiological changes are the result of multiple processes that happen in the brain. Both at the time of the trauma and the secondary effects that may occur minutes to hours after the trauma (Xiong et al., 2013).
Animal models have been used for several decades for the study of TBI. TBI pathophysiology has been studied in cats, rabbit, dogs, sheep, rats, mice and pigs. But more and more researchers and clinicians are using mice and rats extensively (Commission, 2010). This is because humans share about 99 % of a rat's genes, which makes rats eligible when using a model organism to examine human diseases or induced injuries (Lavine, 2002). Rats as organism models are also cost-efficient, easily available and speed up the research because of their shorter lifespan (Commission, 2010). Since rats are getting more common in research for the human nervous system it is important to understand the similarities and differences between rat brains and human brains (Miller et al., 2010).

1.3 The difference and similarities between humans and rat models

There is always a difference between the target and the animal used. One reason is that injuries in animal studies differ compared to the accidents that typically cause human injuries, since the animals are usually harmed using different methods. This is both beneficial and a cause of problems. It is beneficial since this means that the injury can be isolated, and problematic because it is not transferable to humans without modifications. Other differences such as injury volume, axon density and other structural differences are relevant to consider when comparing the results from animal studies with humans. Another difference is that in the case of the rats we know their genetic background and can produce relatively homogeneous

types of injuries. Where as with humans preexisting factors and conditions such as medication, alcohol or genetics can affect greatly when scanning for an acute injury (Xiong et al., 2013). These conditions might be a contributing factor to their injuries and can affect the results.
There are also differences in anatomy and biomechanics when using models based animals, that need to be accounted for. One of the differences in rats, is that the rat brain is located within a elongated skull. Because of that, the brain injuries may be caused in different regions compared to humans (Zhang et al., 2014).

1.4 Conventional imaging technologies to detect brain injuries

There are several different imaging technologies that can be used to visualize different types of brain injuries. One of the most conventional method used today is CT. This section will cover the advantages and disadvantages of the two most conventional methods, namely CT and MRI. The coverage will include such as how they work, how the images are acquired and what they detect. This will be followed by Diffusion Tensor Magnetic Resonance Imaging (DT-MRI) which is a further development of MRI that is especially suited for creating contrast between white and gray brain matter. There are several other protocols for MRI that can be used for creating contrast in the brain, such as functional MRI, but that is typically measured on subjects that are alive while they are performing some task and registering the response in the brain. Since the images were taken ex-vivo, this was not an option here and while it could still be interesting for clinical purposes, it was considered outside the scope of this thesis since it could not be applied to our dataset.

1.4.1 Computer tomography

A CT consists of a X-ray tube and detector array. It measures X-rays traveling through the patient from different angles. The contrast is created by examining the cross-section from the X-ray beams in the tissue. Seven generations of CT scans exist today, and each differs in the relation between the X-ray beam and the detectors. The different geometries between the X-ray beams are parallel, fan, helical and cone. The problem with the first generations of CT scans is that the scanning times required were to long which led to motion artifacts. To avoid the artifacts, faster CT's have been developed. For some machines it takes about 1000 milliseconds to scan and reconstruct an image and the spatial resolution in conventional CT scanners is usually around 1-2 mm, but in more advanced machines it can be even lower, but then a longer imaging time is typically required and are not usually used clinically (Ketcham and Carlson, 2001)(Prince and Links, 2006). Because of the short time, the patent can now hold its breath to reduce motion artifacts even further (Prince and Links, 2006).
CT is often use to produce detailed images of the different organs. Its effective when it comes to determine different injuries such as brain hemorrhages, but it's limited when it comes to detecting AI and other injuries in milder cases. In fact, according

to Lee and Newberg (2005) studies have shown that CT only detects injuries in these milder cases around 10% of the time, and only 1% require neurosurgical attention. Since the injuries studied in this thesis could be considered to be mild, CT is likely not the most effective way of detecting injuries, especially since CT is not ideal for creating contrast within tissue. However, it is very good at creating contrast between tissue and dense materials such as bone. Another, possibly more useful, method for detecting AI is MRI.

1.4.2 Magnetic resonance imaging

MRI works by measuring the magnetic resonance in atomic cores. This is not measured directly, but it can be measured indirectly. The most common atom to examine in the body is the ordinary hydrogen atom, which is prevalent throughout the entire body due to the high water content.
Hydrogen atoms, and other nuclei that have a spin, posses a microscopic magnetic charge (Prince and Links, 2006). When an external magnetic field is applied, the magnetic charge of the atoms begins to align with the external field. When the magnetic field is applied the magnetization of the the atoms will precess around the direction of the applied magnetic field. The magnetization can then be split into two parts - a longitudinal one and a transverse one. The longitudinal part of the magnetization is aligned with the applied field, whereas the transverse magnetization is described by both of the two orthogonal components. The actual signal output is the result of Faraday induction - the fact that a magnetic field varying due to the precession across a coil of wire will induce a voltage. By placing a coil close to the machine, this can be measured directly (Prince and Links, 2006).
The next step is applying oscillating magnetic pulses perpendicular to the static field, which makes the atoms change away from the aligned position. When removing the pulses, the nucleus relax into their original position. It is the changes and differences in relaxation time that form the basis of MR imaging (Martin, 2009).
The most common parameters recorded are called T_1 and T_2, where the former of these is longitudinal relaxation time. It describes the longitudinal magnetization as it returns to the equilibrium position after applying the magnetic pulses. The latter parameter instead focuses on transverse relaxation, measuring the time it takes for the pulse to decay (Prince and Links, 2006). As explained, MRI focuses on the measurement of water molecules. If two different sets of tissue contain an approximately equal amount of water, it is impossible to distinguish between them using conventional MRI. This has lead to different variations in how you process the signals in order to create contrast between tissues and for the separation of gray and white brain matter DT-MRI has shown promise.

1.4.3 Diffusion tensor magnetic resonance imaging

To explain the DT-MRI method one must start with Diffusion Weighted Magnetic Resonance Imaging (DW-MRI). As the name suggests it weights the contrast of MR images dependant on diffusivity. As mentioned the measured MRI signal is commonly obtained from water molecules.

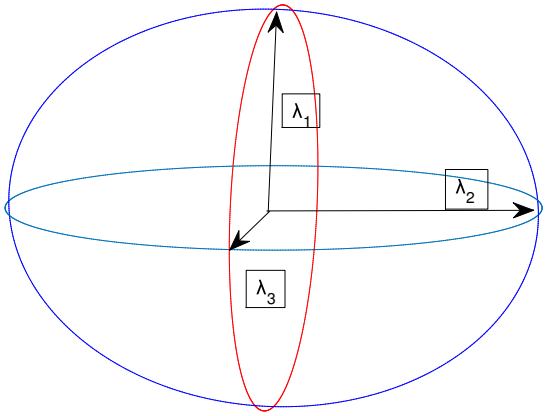

Figure 1.2: Ellipsoid displaying diffusivity, where λ_1, λ_2 and λ_3 are the different radii, and in this case it is isotropic which means that λ_{1-3} are all equal.

Water molecules, when unhindered, will diffuse isotropically, i.e. equal in each direction. The conventional MRI method applies one pulse sequence, where as by applying a second magnetic pulse delayed by time t, it is possible to generate a diffusion encoding gradient (Hagmann et al., 2006). A single DW-MR image is the result from applying one gradient and recording the image this produces.

By recording several DW-MR images with different gradients it is possible to calculate a tensor matrix that describes the diffusion in axis corresponding to the MR-machine. The resulting tensor D is shown in equation 1.1. The diagonal entries are the principal directions of the machine. There are six unique values to the tensor, which is also the minimum required amount of gradient directions for performing a DT-MRI scan. The values correspond to the measurements from six different gradients and an ordinary T_2 weighted image without any gradient weighting, also known as b0.

$$D = \begin{bmatrix} D_{xx} & D_{xy} & D_{xz} \\ D_{xy} & D_{yy} & D_{yz} \\ D_{xz} & D_{yz} & D_{zz} \end{bmatrix} \tag{1.1}$$

By calculating the eigenvalues and eigenvectors of the D matrix, the result can be further evaluated.

It is not always certain that the principal direction of diffusion is aligned to the axis of the machine. By calculating the eigenvalues (λ_1, λ_2 and λ_3) with eigenvectors v_{1-3} the magnitude of the principal directions of diffusion and their orientation in relation to the base system is acquired (Mori and Zhang, 2006). An illustration of the eigenvalues can bee seen in figure 1.2.

These eigenvalues can be used to create other indicators, including the commonly used Fractional Anisotropy (FA) which is a measurement of the degree of anisotropy and is a scalar value between zero and one. A value of zero indicates that the diffusion is equal in all directions, while a value of one indicates that the diffusion is entirely in one direction. One way of calculating FA is given by Kumar et al. (2009) and is shown in equation 1.2:

$$FA = \frac{1}{\sqrt{2}}\sqrt{\frac{(\lambda_1 - \lambda_2)^2 + (\lambda_2 - \lambda_3)^2 + (\lambda_1 - \lambda_3)^2}{\lambda_1^2 + \lambda_2^2 + \lambda_3^2}} \tag{1.2}$$

FA can be an interesting measurement when examining brain injuries, especially when examining regions of white matter since they consist primarily of axons. These are nerve fibres that are anisotropic due to their myelin sheath that limits diffusion in directions that are not perpendicular to the fibres (Oxford University Press, 2010).

The primary direction of anisotropy, commonly called the axial direction, is given by the first eigenvector and its magnitude by the eigenvalue, λ_1. Using a selected region of the brain for seeding it is possible to follow the direction of the diffusion and retrace the fibers. This operation is called tractography and can be performed through different tracking algorithms and methods (Hagmann et al., 2006).

DT-MRI has become more common for clinical use, especially for studying different neurological regions. It has been shown that FA may be a good tool for evaluating the healing process of axons over time, which has been attempted in the spinal cord (Bazley et al., 2012). State of the art MR-machines for animals typically have around 9 T field strength, whereas clinical machines are around 3 T. The spatial resolution is as such typically lower in clinical settings, usually around 2-3 mm for each dimension (Jones and Leemans, 2011). Given that this is larger than an individual axon, DT-MRI will not be able to resolve individual axons, since each voxel is a mean value of all of the tissue contained within. Machines with higher field strength can acquire smaller voxels, and when imaging for longer times and averaging is used small voxels can be imaged. Exactly how small voxels that can be resolved varies on the time available, but studies have shown images that appear to have acceptable SNR with voxel sizes as small as 0.00024 mm^3 as early as in 2002 (Benveniste and Blackband, 2002), and it is likely that with improving protocols and underlying technology the spatial resolution will continue to become smaller. The interest in DT-MRI has grown over the last decade, but there is not a gold standard for what values are classified as normal within a brain (Hulkower et al., 2013). As such, most studies use control sets to compare findings to, just as has been done in this study. Analysing tractographies and voxel-wise analysis are two common methods used, and a common site for findings is within the corpus callosum according to Hulkower et al. (2013), which is a review study comparing several articles regarding traumatic brain injury being examined using DTI. However, the degree of injury is varied and detecting axonal injury is still a major challenge for DTI.

There are several artifacts associated with DT-MRI. Two of the most common artifacts are blood flow and subject movement. These artifacts not an issue in this thesis since the rat brains were fixated. One artifact that could be corrected is Eddy currents. These currents form as a response to oppose the changes in the magnetic field (Smith, 2010). These artifacts show in the form of warping the image along the applied gradient direction.

1.5 Aim

The goal of this thesis is to design a protocol to detect AI in rats from DT-MRI data and are not visible in standard MRI. To realize a protocol, DT-MRI data will be used collected from ex-vivo DT-MRI with and without the rodents being subjected to rotational trauma. Additional data and evaluation beyond what Carcedo performed will be used to develop a protocol. To succeed, different normalization techniques will be evaluated in order to to compare data from different specimens. The possibility of using tractography to visualize the neural tracts and detect the AI will also be examined.

2
Previous Work

In this chapter the work that was done prior to the start of this thesis will be presented in order to provide a background. This includes information pertaining how the data itself was acquired. How the data had been analyzed prior to this thesis by Carcedo (2012) and a separate study performed by Davidsson et al. (2015) on other animals with aim to asses pathology.

2.1 Animal experiments and data

The DT-MRI data in this study was acquired from Karolinska Experimental Research and Imaging Centre (KERIC), in Stockholm. The data consists of 11 sets of DT-MR images from Sprague Dawley male rats, with each scan including a non weighted reference image b0. The 11 subjects were divided into three groups: five exposed, four normal and two sham-exposed, (henceforth referred to as sham). The exposed rats were subjected to rotational trauma to induce a brain injury in 23-07-2012. The sham rats were placed within machine used to generate the trauma, but they were not subjected to any trauma, and normal animals served as reference. The rats were then kept alive for 24 hours before they were euthanized. The brain was removed from the skull and rinsed by transcardial perfusion then fixated for 24h. The brain was scanned in KERIC's Varian scanner from Agilent technologies, with a field strength of 9.4 Tesla and a bore of 30 cm. Different coils can be used to acquire different resolutions and space. The coil used to acquire these images were 30 mm.
The ex-vivo rat brains were placed in the scanner with a regular spin echo sequence TE/TR to produce diffusion weighted images S_x. The diffusion was then measured in 30 directions with one unweighted MR image as a reference. The images produced were 256x256 pixels with a width of 28.8 mm and height of 19.20 mm and the image was divided into 55 slices with a total thickness of 27.5 mm. The specified dimensions then equal 0.11x0.07x0.5 mm per voxel. The b-value, calculated from equation 2.1 given by Le Bihan et al. (1986), was 12500 s/mm^2 with the physical factors: The durations of the pulses $\delta = 2.6$ ms, the time between pulses $\Delta = 9$ ms, the amplitude of the pulses $G = 54.37$ for the two pulses and γ, the gyromagnetic ratio for the hydrogen nucleus 42.58 MHz/Tesla (Boston College, 2015). The data was then used to calculate the diffusion tensor, which could be diagonalized to compute the eigenvalues and corresponding eigenvectors.

$$b = \gamma^2 G^2 \delta^2 (\Delta - \delta/3)[\mathrm{s/mm}^2]. \tag{2.1}$$

Table 2.1: List of all animals that where used for the results. The two sham-penetrated animals where only used for parts of the voxel-wise analysis, and one sham animal was excluded due to the images being taken using a different MRI coil.

Animal	Class	Weight (g)	Rot. Acc. (Mrad/s^2)	Date imaged	Used
E305	Exposed-rotation	414	1,74	20/08/2012	Yes
E306	Exposed-rotation	399	1,83	18/08/2012	Yes
E307	Exposed-rotation	396	1,73	15/08/2012	Yes
E308	Exposed-rotation	428	1,81	13/08/2012	Yes
E309	Exposed-rotation	376	1,87	16/08/2012	Yes
N310	Normal	399	0	20/08/2012	Yes
N311	Normal	412	0	22/08/2012	Yes
N312	Normal	397	0	19/08/2012	Yes
N313	Normal	397	0	24/08/2012	Yes
S314	Sham-rotation	411	0	10/08/2012	No (Different coil)
S315	Sham-rotation	428	0	14/08/2012	Yes
S301	Sham-penetration	432	0	14/08/2012	Voxel-wise only
S302	Sham-penetration	435	0	18/08/2012	Voxel-wise only

Below a table (table 2.1) that contains the different animals that where used for the results of this study are presented. The two sham-penetrated animals where only used for parts of the voxel-wise analysis were sham animals from another study, which examined penetrative wounds. As such they had a surgical hole at the top of their skull bone, but it should not affect the values withing the corpus callosum. N312 was the animal that was used as a template for spatial normalization. Sham animal S314 was later found to have been imaged using a different coil than the rest of the animals, and was excluded from this study for that reason.

2.2 Carcedo's study

Carcedo M. G. examined AI from the same DT-MRI data set that was used here, (Carcedo, 2012). Her work consisted of examining the three primary eigenvalues for one rat and evaluating the eigenvalues relative to each other in the brain. This was done by segmenting the brain into several regions see 2.1. Four different pixels were evaluated. The pixels were extracted from areas A to D in 2.1a, each containing three eigenvalues located in the Corpus Callosum (CC), from two different DT-MR images (slices). The mean of each eigenvalue was also examined in four regions 2.1a of three consecutive slices 2.1b, (alongside the sagittal plane of the brain) in CC, hippocampus, cingular cortex and the pyramid tract.

Furthermore, the work consisted of normalization of the eigenvalues amplitude. The report also pointed out some abnormalities in the images which include white dots, thin white lines and a lighter region, see figure 2.2. The dots in figure 2.2b are likely the result from the cotton layer that was used during the scanning process and it

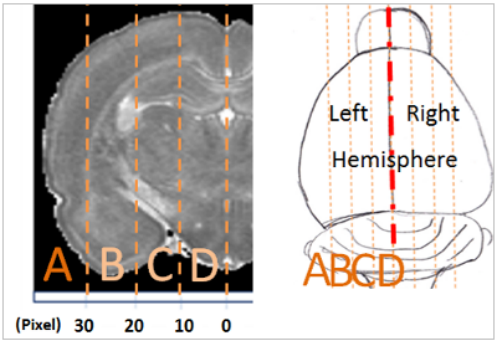

(a) Segmentation for each slice using only the left hemisphere, A-D each with a width of about 10 pixel

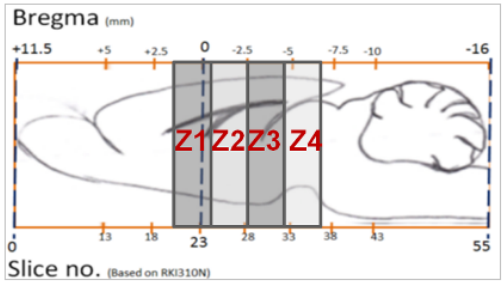

(b) Segmentation for the brain, the segments Z1, Z2 and Z3 containing three slices and Z4 containing four

Figure 2.1: This is the different method used by Carcedo when segmenting the brain into smaller regions

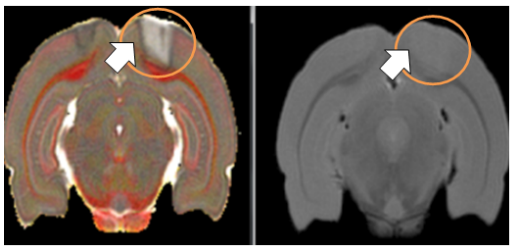

(a) Region containing abnormal values is indicated by the arrow.

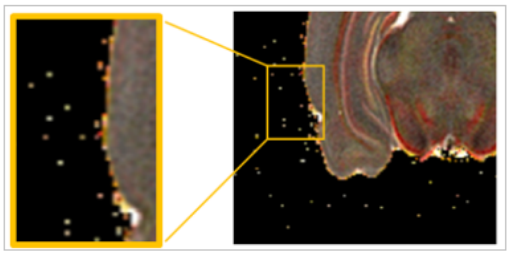

(b) The particles around the subject are likely cotton particles.

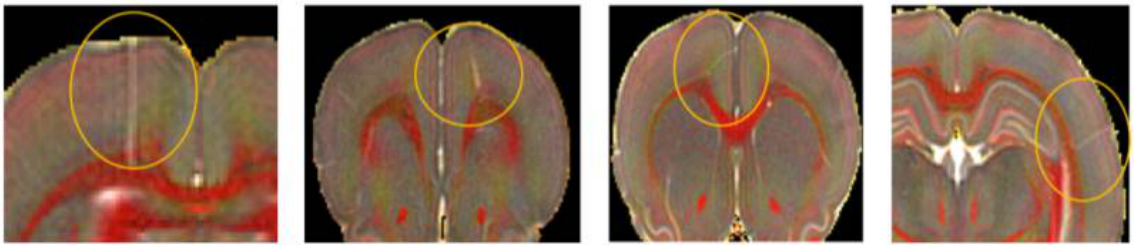

(c) Thin white lines that were not expected.

Figure 2.2: The images display different abnormalities that Carcedo presented, (Carcedo, 2012).

does not affect the values obtained from the brains. The brighter regions, see figure 2.2a were found in all exposed rats, from about -6 mm to -8 mm from the bregma (anterior-posterior) but it was not found in any sham or normal subjects. Because the region was outside of the Region Of Intrest (ROI) and in the gray matter, this finding was set aside by Carcedo. In figure 2.2c the thin white lines that at the time where unexplained are shown these lines will be further explained in section 4.1.

Table 2.2: Eigenvalues for corpus callosum from different area (A, B, C and D seen in 2.1a) and segments (Z1, Z2, Z3 and Z4 seen in figure 2.1b), (mean ± standard deviation). The most significant values are shown below.

Bottom layer CC	λ_1	λ_2	λ_3
Exposed	0.55±0.06	0.33±0.05	0.23±0.05
Normal	0.53±0.06	0.34±0.06	0.23±0.06
Sham	0.43±0.06	0.26±0.08	0.19±0.08
Upper layer CC			
Exposed	0.55±0.09	0.34±0.04	0.22±0.03
Normal	0.54±0.04	0.35±0.03	0.21±0.03
Sham	0.43±0.05	0.27±0.04	0.19±0.03
Mid CC			
Exposed	0.60±0.07	0.27±0.06	0.17±0.04
Normal	0.59±0.05	0.27±0.06	0.16±0.04
Sham	0.45±0.05	0.22±0.05	0.15±0.04

In Carcedo's results, she suggests that most deviations in eigenvalues are found in and adjacent to the CC. One of her important finding around CC is displayed in table 2.2. CC is here divided into three regions: upper, middle and bottom CC. The upper and bottom layer has a thickness of one voxel were the border between white and gray matter and the mid is the remaining pixels in between, see 2.3. When normalizing these value, from table 2.2 the significant changes in eigenvalue also changes from the rear region to the front region. The rear region as she called it, is the CC far from the ventricles and front is closer in one slice. In Carcedo's conclusion it is explained that a spatial normalization of the images should be performed in order to do an comparison between rats. The conclusion also suggest different tools that might be useful in future studies when examining AI such as fibre tracking, FA and apparent diffusion coefficients. For future studies she suggested more normalization: both spatial and intensity normalization, perhaps by using a template. This in order to make the results more robust. She also suggested examining other brain regions containing white matter. The evaluated and the conclusions that were drawn from her work will resume in method section 3.1 and result section 4.1.

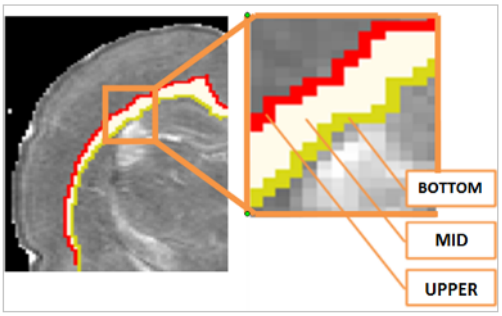

Figure 2.3: The division of CC into three smaller segments to differentiate different regions inside the CC

2.3 Pathology following experimental brain trauma

In a study by Davidsson et al. (2015), AI were detected and presented in images. This detection was done by examining thin slices from a rat brain stained by antibodies, under microscope. The rat brains used were not those used in this study, but was similar in breed and age and subjected to similar trauma.
The main result from the study is shown in figure 2.4. The reference point used was bregma. To be able to locate injuries from the DT-MR images in this thesis, the focus will be on the sites of injury. Which are marked by stars in figure 2.4. Special attention will be in the CC region

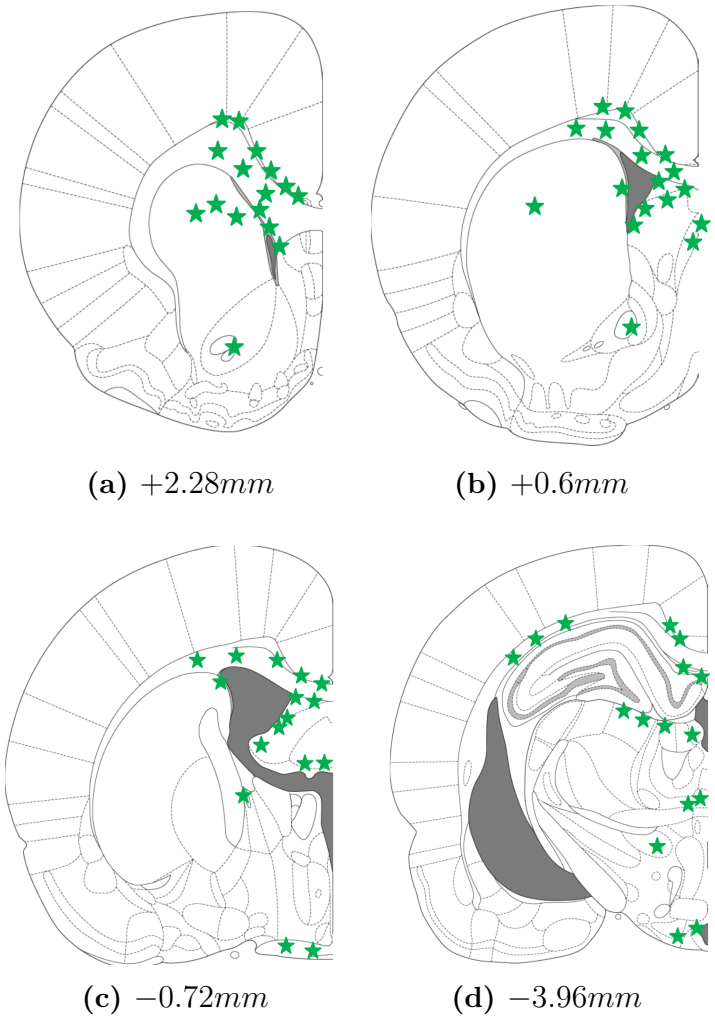

(a) $+2.28mm$ **(b)** $+0.6mm$

(c) $-0.72mm$ **(d)** $-3.96mm$

Figure 2.4: The images display injuries seen at different distances from bregma (Davidsson et al., 2015)

.

3
Methods

The following chapter presents the data processing. The primary software used was MATLAB R2014b (Mathworks). ImageJ 1.48h3 (National Institutes of Health), ScanIP v.5.1(Simpleware Ltd.) and DSI-Studio (17 Dec 2014 build) have also been used with various amounts. Since the goal of this thesis was to detect differences between the different sets of animals without any clear preference for certain methods, several different methods were attempted.
Axonal injury is characterised by an initial axonal swelling, followed by the axons themselves disconnecting (Siedler et al., 2014). This thesis has worked under the assumption that axonal disconnection would lead to water flow becoming more isotropic locally around injuries. If this is true it would lead to the smaller eigenvalues getting closer to the largest eigenvalue resulting in a decrease of fractional anisotropy compared to healthy animals, whereas the sum of the eigenvalues is difficult to predict: there could be a decrease in the primary eigenvalue that offsets the increase in the other two, causing no effective change, or it could increase if the primary value remains constant and the other two increase. From this the assumption that results could be acquired in two major ways was formed: Either individual voxels could contain drastically different values compared to other animals, or there could be small minute changes across a larger region that is very difficult to detect when just comparing values, but a classifier could perhaps be utilized to detect such trends when comparing between normal and exposed animals. In figure 3.1 an illustration of how these two sorts of injuries could be looked at is presented: The lighter colored region represents the regional injuries and the lone dark red point indicates an highly differentiated value compared to the surrounding tissue.

Figure 3.1: Sketch of the corpus callosum illustrating the two expected types of injury: Either isolated points that differ greatly from the surrounding tissue, as illustrated by the isolated dark red point, or a more regional change in values, that might be difficult to detect using a voxel-wise .

3.1 Analysing results from Carcedo

The primary method for evaluating Carcedo's results was to examine the methodology and verify the methods from a theoretical view: Are the results reasonable and can the conclusions that were drawn be supported by the data. Carcedo's two main methods were the following: Manually identifying regions and semi-automatic detection, and they where both studied. Her findings seems credible and therefore no verification of her results was performed.

3.2 Relating slices to bregma

A method to relate the position of specific MR-DT images to bregma was developed. This method provides a look up table. This to be able to compare findings in the rat brain with future studies. Images from the animal were correlated to the atlas from Paxinos and Watson (2009) and the points where different anatomical regions split up where chosen as references as they are clearly visible. Four different regions were chosen: two were CC changes splits into forceps major and minor, bregma 0 and the end of the image set. The thickness of the slices makes it difficult to exactly pinpoint where in relation to bregma an image is, so all values are approximations that can vary up to 0.2 mm.

3.3 Image reconstruction and removal of artifacts

For each rat there were 31 different sets of images, each with 55 slices. One of these sets was without diffusion weighting b0, while the other 30 were evenly spaced gradient directions. In order to create a DT-MRI from these, several steps needed to be considered. It was possible to set up a method as done by Kingsley (2006):

$$Y_i = \ln(S_0/S_i)b \tag{3.1}$$

Y_i is the apparent diffusivity constant for each gradient weighted image, normalised by the unweighted image and b is the value specified earlier see equation 3.1. S_0 is the b0 image set, and S_i is one of the gradient weighted image sets.

$$H_i = \begin{bmatrix} g_{xi}^2 & g_{yi}^2 & g_{zi}^2 & 2g_{xi}g_{yi} & 2g_{xi}g_{zi} & 2g_{yi}g_{zi} \end{bmatrix} \tag{3.2}$$

H_i is a matrix created by the gradient weighting of each of the images. Both of these will, for each voxel of the images, construct an Mx6 matrix, where M is the amount of gradient directions. When M=6 an exact solution can be calculated from the following equation 3.3:

$$Y = Hd \tag{3.3}$$

Where d is a vector containing the six unique elements of the diffusion tensor, see equation 1.1.

$$d = \begin{bmatrix} D_{xx} & D_{yy} & D_{zz} & D_{xy} & D_{xz} & D_{yz} \end{bmatrix}^T \tag{3.4}$$

So in the case of M=6, d can be calculated by equation 3.5

$$d = H^{-1}Y \tag{3.5}$$

In most cases when DT-MRI is used, more gradient directions than six are used in order to improve the signal to noise ratio and account for diffusion in more directions. In such cases reconstruction can be done using different methods. The method used in the reconstruction was an unweighted linear least squares approximation. By forming a pseudoinverse through multiplying H with it's transponate, equation 3.6 is setup.

$$d = (H^T H)^{-1} H^T Y \tag{3.6}$$

Once this was performed its possible to directly calculate the eigenvalues and eigenvectors of the diffusion tensor in each voxel of the image. Further some artifact correction needed to be performed, because the images were shifted slightly because of the non homogeneous magnetic field created as a result of the added weighting. This is called Eddie currents. There are different methods for correcting the influence Eddie currents on the resulting images, but since the data at hand had already been collected, focus was placed on post-processing correction methods.
One method described by Mohammadi et al. (2010) suggests that registering each gradient measurement series onto the unweighted base image prior to reconstruction can counteract the Eddy current efficiently. This was performed in MATLAB by applying an affine slice-wise image registration of each gradient image onto the corresponding unweighted image.

3.4 Region extraction of corpus callosum

Regions of interest of the rat brain were extracted. Since AI was the main focus, regions made of white matter was an obvious choice because it consists mainly of nerve fibers. One important area which consists primarily of white matter is the Corpus Callosum (CC). The aim was to extract the CC from the rest of the data, with the added goal of performing the extraction without utilizing the data that would primarily be used for evaluation of the presence of AI. Hence, images without any gradient weighting information was used, the b0 images. The CC was discernible from the other parts of the brain, and an algorithm was developed that extracted the corpus callosum.
The algorithm was based partly on dynamic programming, during which the cost of traversing each pixel from one side of the image to the other was calculated based on edges and the intensity in the image. This was done by normalizing the image intensity to lie between the range of 0 and 1 and edge features in the image where calculated using two sobel operators, with a weighting of 1.5 for the gradients alongside the vertical line and 0.5 along the horizontal line. After calculating the cost for each voxel the cheapest path along the coronal plane was calculated. The cost matrix was tuned so that the path followed the CC by adjusting the intensity and edge weighting, i.e. a scaling on each of the parts of the cost matrix to tune the resulting cost for each voxel.

After the line was established the median and standard deviation of the values in the original image along the line were calculated. The median value was chosen over the mean since the majority of all points are expected to be within the CC and thus are white matter, causing the median to be more representative for the white matter values than the mean, which would also include gray matter. Points above and below the line were examined and if they fell within a tolerable interval they where added to the mask, a binary image that can then be multiplied with other parameters in order to extract the region of interest. The interval was between 0.01 (i.e. 1% of the maximum value of the b0 image) and the median value with 1.8 times the standard deviation added. The lower bound was chosen to be very low since the b0 images that where used as input typically have lower values in the corpus callosum than the surrounding gray matter, whereas the upper bound was chosen experimentally to include some gray matter, while not extending too far from the CC. Points not on the line, but above or below it, had an additional smoothing term applied which was the amount of pixels away from the line multiplied with a seventh of the std, making it less likely to include pixels the further from the line each pixel is. These values where all taken experimentally after trying several different variations. By performing these steps on each slice a 3D mask and then multiplying the binary mask with the region of interest can be extracted from each parameter.

A mask was also made by hand, for slices between bregma 2.52 and bregma -5.4 where the majority of the CC is. The mask extended a short distance out into the gray matter. This was done in order to be able to use a mask that included a controlled amount of gray matter surrounding the CC. The mask was created in MATLAB using a function, roipoly, that created a mask within an area that was drawn directly within the images.

3.5 Evaluation of techniques for processing data

There are several ways that DT-MRI data can be processed and handled to generate meaningful results. Some of these techniques depend on calculating different parameters from the eigenvalues, such as FA. Others, like tractography, use FA to track the fiber orientations. In this section the methods used to evaluate the usefulness of these tools are described.

3.5.1 Evaluation of fractional anisotropy

The usefulness of FA for detection of injuries was examined by studying equation 1.2, the equation used to calculate it, presenting different strengths and weaknesses that are inherent with the method that is used to calculate FA. Furthermore, a set of images that show an incident where FA, inside the CC, does not show changes that is visual in the eigenvalues. Calculations of FA images was also performed using the equation 1.2

3.5.2 Evaluation of tractography

Tractography and it's strengths and weaknesses are presented together with a tractography that was carried out using DSI-Studio (17 Dec 2014 build); First DSI-Studio masks the brain from the background. Secondly, in this study the whole CC was traced by hand and set as a ROI, and tractography was then performed with whole brain seeding and set to only include fibers that passed through the region of interest. The standard settings for stopping were used, 0.08 FA and an angular threshold of 50°.

3.5.3 Evaluation of the mean and standard deviations of eigenvalues

The standard deviations for the three eigenvalues and the FA were calculated for the whole brain of each animal. That is to say, that the mean and standard deviations of the entire brains were calculated after performing the artifact correction. This was done using MATLAB.

3.6 Spatial normalization

To be able to compare diffusion at a voxel by voxel level a voxel-wise spatial normalization was performed in multiple steps. First, the subjects where registered onto a template (one of the normal animals with few imaging artifacts was chosen, animal N312). They were registered using 3D affine registration that allowed for translation, rotation, scaling and shearing, using the function *imregtform* from MATLAB with an initial transform that only allowed for translation, rotation and scale, with a growth factor of 1.05, epsilon of $1.5e^{-}7$ for a 1000 iterations. This was followed by the full affine registration, that had a growth factor of 1.01 and went on for 20000 iterations. The registration was performed on the b0 images and the translation matrices for these cases were then used to transform the DT-MRI reconstructed images such as FA.

Second, attempts were made to estimate displacement fields that could further map each of the brains onto the template. This is a delicate step where using too few iterations could result in an erroneous mapping and distort the data. The displacement was calculated for each brain separately, generating a unique displacement field for each brain. All fields were, however, calculated in the same way using the same parameters and MATLAB function: *imregdemons* at three pyramid levels of 3000, 1000 and 600 iterations respectively with a smoothing factor of 1.3. This displacement was calculated on FA maps that had been registered using the affine translation calculated on b0 images. This because the b0 images are not affected by the eddy currents. The target image was excluded from all the following examination were the images are aligned, in order to only compare data that had been processed in the same way.

3.7 Voxel-wise analysis

After performing the affine translation and displacement, as presented in section 3.6, the mean and std of each voxel for all of the normal animals was calculated. To create a stronger normal reference to compare the injured animals with. By comparing the value of each voxel with the corresponding mean value and standard deviation, the goal was to find pixels that are significantly lower in value than the mean value. Since it would be expected to find lower FA values in injured animals then in normal animals.
This can be described as in equation 3.7 where $FA_p(x, y, z)$ is the value of the animal being examined in the point x, y, z and FAmean(x, y, z) and FAstd(x, y, z) are the mean and standard deviation values of the remaining normal and sham images in the same point (so when examining an exposed animals all normal and sham animals are included in the mean and std, but when each normal or sham animal was examined it was excluded from the mean and standard deviations of each voxel).

$$FA_p(x, y, z) < \text{FAmean}(x, y, z) - 2 \cdot \text{FAstd}(x, y, z) \tag{3.7}$$

For the voxels where this were true, the voxels were flagged as being of interest. These points were displayed in the animal, after removing all points that were not within or close to the CC. This produced a visual display of each point that was marked as interesting, but a count of how many points within the CC for each slice was also calculated.
In order to improve the results from this analysis, more samples in the normal group would be valuable. As it turns out, a different study had been performed using the same MRI settings, but a different trauma. This still allowed for using the uninjured animals from that study to increase the amount of normal animals available for this comparison. As such two additional animals were added, and used in the mean value and std calculations (except for their own comparisons, following the same procedure as before). It could be possible to include the exposed animals in the mean value, but they where kept separate. This to remove the possibility of the injuries being obscured by the mean value, should the injury be located in roughly the same place in all injured animals. The additional animals used to get a more significant mean value.
Since these images were not amplitude normalized in any way, performing such a normalization was a possible way to improve the results. As such, the histograms of each volume was matched with that of with the target animal, using the MATLAB function *imhistmatch*, which could possibly resolve issues such as differing perfusion by evening out the different levels of values and normalizing the amplitude. This was performed after the affine registration, but before the displacement fields where calculated, since it seemed likely that improved matching between the animals would improve the performance of the displacement field algorithm.
Overall, the process followed can be described with a flowchart, shown in figure 3.2

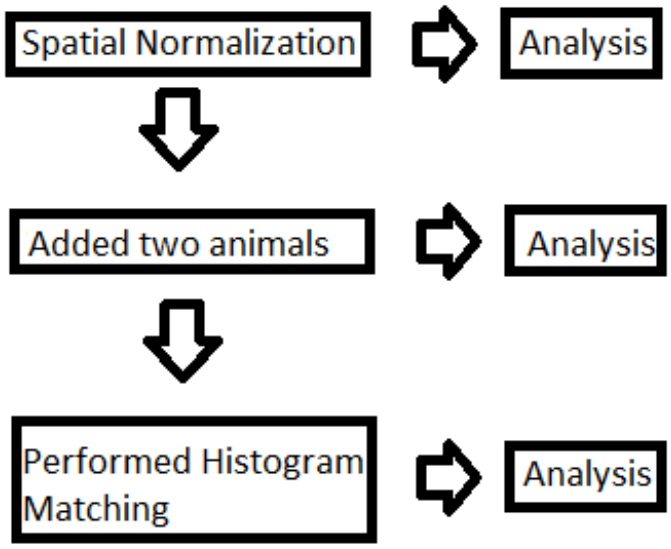

Figure 3.2: Flow chart of the process that went into refining the results from the voxel-wise analysis. Spatial normalization includes translation, rotation, scaling and shearing as well as applying the displacement field.

3.8 Examining voxel values within corpus callosum

Other methods for comparing the values within the CC were used as well. The focus in these methods was not placed on each individual voxel but rather on trends within all of the voxels within the CC. In this section these methods are presented.

3.8.1 Examining trends within subjects

Changes within CC when examining three adjacent slices were examined by approximating the overall shape of the CC and then checking the changes in prior diffusion values alongside this direction, see figure 3.3. When comparing within the same animals and its slices, pixels can not just be compared between different slices because CC is not straight. This was further expanded on to include all gradient directions and checking each of them for changes. This is expanded upon in the following part bellow.

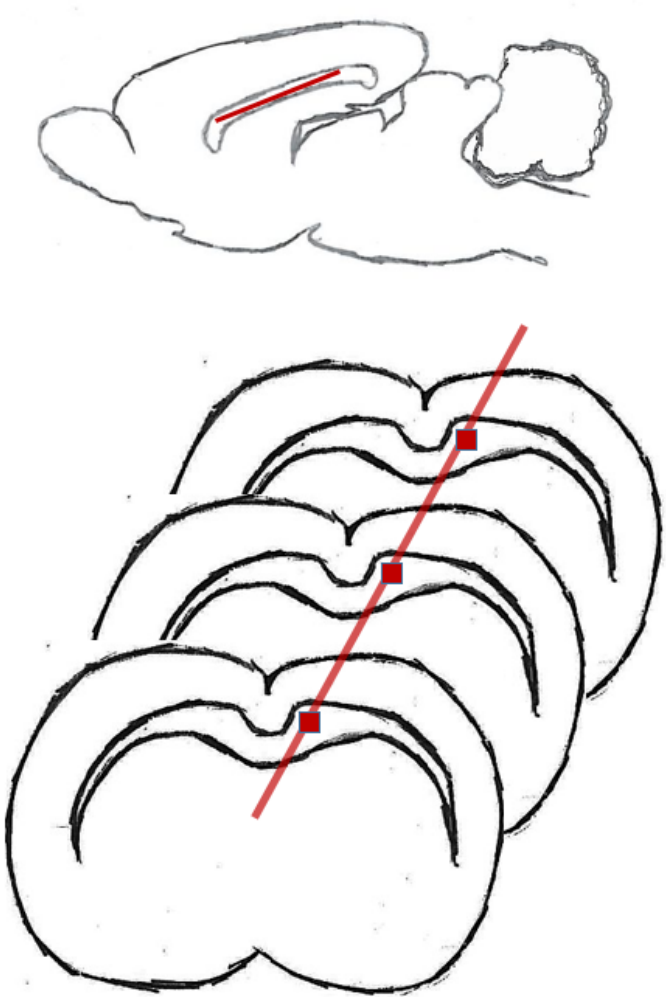

Figure 3.3: The top image displace the rat brain in a frontal view and the bottom images the pixels extracted out of each slice.

3.8.2 Examining trends within all gradients

A more complex method for examining the difference in values of each of the original gradient directions was also tested: The different gradient directions from the weighted gradient data were evaluated to check for differences in the gradient directions between normal and exposed. The data was tested in the three following ways:

1. Evaluating distributions of values using so called cluster analysis, to examine if the exposed and normal animals diffusion values differs. A distinction could be elevated diffusion values in normal animals compared to exposed.

2. Examining the mean value of each diffusion direction for ten consecutive slices inside CC, from about bregma 2.52 to bregma -5.4.

3. Aligning the animal, examining each diffusion value inside CC and calculating the mean value of each slice for ten consecutive slices, from about bregma 2.52

to bregma -5.4.

The so called cluster analysis, mentioned in item 1 of the above list, was performed using neural clustering, one of MATLAB's built in functions in its neural network tool box. Neural clustering groups data by similarity by using weight and bias learning for each batch. The amount of neurons decides how big the two dimensional self-organizing map will become. 30 neurons were used as in the example shown in figure 3.4. The default is 10 neuron but because of the large data sets 30 neurons were chosen. One neuron contains weight and bias to asses the input data. More information about neurons will be presented in section 3.9.2. Each self-organizing map shows the weights from each neuron and each input. The difference to classification, which will be covered in section 3.9, is that clustering does not know which animal is which. Clusterings goal is to find hidden patterns or structure within the input data. More information about clustering can be found at MathWorks.[1]

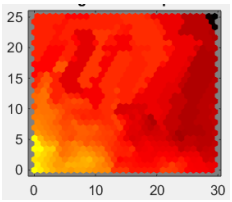

Figure 3.4: the image displays an example of a 30x30 self-organizing map, shown on the axis, from one input. The image created by MATLAB toolbox is misleading since both axes should be 30, corresponding to the amount of neurons used. The strongest connection, weight of one neuron, is shown as red, zero-connection is shown as black and yellow the weakest nonzero connections.

Mean value analysis, mentioned in item 2 of the previous list, for each slice were calculated using the same mask on all animals, for different parameters. The same mask was used in order to get the same amount of pixels and region for each animal, which should be the same region due to the affine registration. This was examined on the FA values of the fully aligned animals as well as when only the affine registration had been performed, and on the different gradient directions with the affine registration applied.

3.9 Categorization of exposed animals using classification

Classification is a tool that can be used to attempt to differentiate between groups of data using some of the data for training and then attempting to decide what kind of data an unknown sample, the remaining part of the data, is. The tool has different requirements on the input in finding patterns, depending on how the classifier works. A general requirement in order to be statistically significant is a decent sample size. In this case the input data is the diffusion and FA data sets and the goal

[1] http://se.mathworks.com/discovery/cluster-analysis.html

is to separate, that is, classify the exposed ones and the healthy ones as different groups. The classification is generally based on finding patterns that distinguishes the different groups of animals from each other. The two different types of classifiers that were used were MATLAB's discriminant analysis classifier with K-fold stratified cross-validation (*classify*) and neural networks pattern recognition (*nprtool*). These methods will be explained in more detail in the following sub-sections.

3.9.1 Discriminant analysis classification

To be able to use the discriminant analysis classification in MATLAB, the data needs to be divided into training sets and test sets. This division is done using a K-fold stratified cross-validation where the data is divided into K-subsets and a value out of each subset is randomly chosen as a test set. The other data is then divided into subsets and run in the classifier k times as training data. The goal is to predict the test data from model derived out of the training data.
The MATLAB function that was tested was *classify*, a Naïve Bayes classifier which means that it is based on Bayes theorem, see equation 3.8. This method was chosen because of the size of the data sets tested. The Naïve Bayes classifier establishes its posterior probability on its previous experience. The classifier used in MATLAB is a diagquadratic one that is based on the following reports: Krzanowski (2000) and Seber (1984). It fits each group using a diagonal covariance matrix estimate from multiple multivariate normal densities (Vikramkumar et al., 2014).

$$P_1(c|x) = \frac{P_2(x|c) \cdot P(c)}{P(x)}$$

For n posterior Probability:

$$P(c|X) = P(x_1|c) \cdot P(x_2|c) \cdot ... \cdot P(x_n|c) \tag{3.8}$$

3.9.2 Neural network, machine learning

MATLABs built in function neural pattern recognition was the second tested classifier used in this thesis. It's constructed in a way that it takes data and creates a network of neurons compatible to the problem to be solved. To optimize the networks performance, the neurons weights and bias need to be tuned. This tuning is the training of the network and require example data. The testing on the network is also validated for each testrun to check its performance. The following equation displays a example equation for a single-input neuron (Beale et al., 2015).

$$a = f(wp + b) \tag{3.9}$$

The weighted input(wp) and bias(b) are both adjustable scalar inputs. In this case b can be seen as shifting f, the transfer function, to the left. There are multiple different configurations of weighted input and transfer functions. The net input, to the transfer function, have two configurations: either a product between the weighted input and bias or like in equation 3.9 a sum. Multiple neurons are used to create a network with desired behavior by adjusting the scalar inputs. The

network contains several neurons which alter the equation into vectors or matrices. The neurons used in neural network can be manually changes but has a default of ten neurons. In our case, the network training with example data uses scaled conjugate gradient backpropagation, to update the weight and bias values (Møller, 1993). There are two different ways to train: incremental and batch. In most cases incremental training is slower and produces more errors than batch training. Batch training was used here and as its name suggests, it adjusts the scalar inputs first when all the inputs and targets are presented (Beale et al., 2015). Training keeps running until one out of five criteria have been met. These are the criteria (Møller, 1993):

- Reaching the maximum number of repetitions, 1000 iterations.
- Reaching the maximum amount of time.
- The performance goal is reached by minimizing the cross-entropy.
- The performance gradient falls below its minimum threshold.
- Validation of the network has increased more times then it has failed.

In the general user interface for the neural network the criteria are set on: 1000 iterations, no time limit, the cross-entropy decrease from 0.514 to 0, Gradient starts from 128 and ends with 1e-6 and six validation checks. All this was done using the general user interface of neural networks.

4
Results

In this chapter the results obtained throughout the study are presented. The results follow the structure of the methods 3.

4.1 Analysing results presented by Carcedo

In the following subsections the results from the analysis of Carcedos study is presented, divided into two parts matching the two different methods used in Carcedos study.

4.1.1 Manually identified regions

The work performed by Carcedo is relevant to this thesis when learning about the animal data and the process of obtaining data. Carcedo worked in maps where the eigenvalues have significant changes of the diffusivity mean. These maps were examined and were intended to be useful as a guideline to localize injuries, but the small differences between normal and exposed animals, as was shown in table 2.2, makes it difficult to use these results. There were very slight changes between exposed and normal animals in the eigenvalues. There were statistical t-tests computed where the result showed that the data can be classified as normally distributed.
There are however some questionable comparisons of the eigenvalues and the way that the data has been segmented into regions by combining multiple slices. The comparison could be misleading in the way that the voxels being compared might not be aligned between animals. Measured coordinates are taken at a fix distance from bregma, presumably taken by comparing the image sets to an atlas. They do not account for the fact that the brains differ in size and shape from one another, and the distance between two voxels in two brain sets may not be the same for all animals. This may lead to comparing the values of two different voxels which would be misleading. A better way would be to have a distance relative to specific features of the brain, or performing a spatial normalization before comparing individual voxels.

4.1.2 Semi-automatic detection of brain regions

The Semi-automatic detection and extraction of the brain regions was performed in Scan IP. These extracted regions appear to be well-fitted to their respective brain regions since after performing an automatic segmentation (thresholding) they were

manually edited to better fit. The values extracted where the eigenvalues, λ_{1-3} and their means within some fairly large regions: Most notably the upper and lower edge of the CC and the body of the CC within the edges. The standard deviations and peaks that were larger than two times the standard deviation. Small differences were found in the mean values of eigenvalues in different regions when comparing exposed, control and sham animals. In fact, the largest differences were typically found when comparing sham with either the normal or the exposed animals. While the exposed and normal animals were similar to each other (though the exposed tended to have larger standard deviations). There was a small amount of sham animals (only two). Statistical analysis on such a small dataset has difficulties in accounting for outliers. Carcedo did not account for one of the sham animals being imaged with another coil, as will be shown in section 4.3.
Amplitude normalization was performed as described in section 2.2 and the results before and after this spatial normalization were presented. There are some things to consider about this normalization: To begin with, it is not entirely certain that the area chosen is unharmed in the exposed animals. This could cause errors to be obscured or highlight parts that are not actually injured.
The main conclusion from Carcedo's work is that normalization, both spatial and amplitude, will be required in order to produce reliable results. This is necessary to be able to compare exposed and non exposed animals directly. This could also open up detection of other regions damaged by the trauma. The conclusion mentions other parameters that could be interesting for further studies such as FA and the apparent diffusion coefficient but the work never addresses them as a solution for finding AI. It also mentions fiber tracking which with the data Carcedo used would not be possible, since it lacked the eigenvectors, which are necessary for tracking the direction of the fibers. With the extended data it is possible, although not necessarily useful, to perform a tractography.

4.2 Relating slices to bregma

In table 4.1 we see the result of comparing our image sets with an atlas. It gives an approximation of what features can be expected in each slice and a fixed reference that could allow for comparisons with other studies

Table 4.1: Table relating slices to distances from bregma. Each slice has a thickness of 0.5 mm, so from these points the distance a slice is from bregma can be approximated.

Slice	Distance from bregma (mm)	Comment
Slice 20	2.52	gcc splits into fmi
Slice 25	0	Slice closest to bregma
Slice 35	-5.4	scc splits into fmj
Slice 55	-15.48	End of image set

gcc = genu of the corpus callosum, fmi = forceps minor or the corpus callosum, scc= splenium of the corpus callosum, fmj = forceps major of the corpus callosum

4.3 Image reconstruction and removal of artifacts

The Eddy currents were corrected for by the method described in section 3.3. An example of the result of correction is shown in figure 4.1. It displays the difference between a gradient weighted image before and after correction.

Figure 4.1: Shown here is the difference between a gradient weighted slice before and after Eddy correction.

Some abnormalities were found, such as black holes, white lines and rings on the edge of the brain. There was also something strange with one of the sham animal images. The images seemed blurrier then the rest of the images, see figure 4.2a compared to figure 4.2b.
When looking into the images specifics a change of coil to 40 mm, instead of the 30 mm that was used to produced all other images was noted. Because of the coil change, the pixel values changed as well and therefor it was decided to leave out this sham animal and examine the ten other animals. The smaller coil should in theory produce results with a higher SNR.
Another abnormality was black holes, one example see figure 4.2c. These holes are probably fomblin that has leaked into the cerebrospinal fluid inside the ventricles. Fomblin is the substance used to create contrast between the background and the object in the scan. The white lines mentioned above, seen in figure 2.2c, and described in the report by Carcedo in, presented in section 2.2. These white lines are probably also an caused by fluid, but in this case inside veins.
Gibbs ringing is an error, shown in figure 4.2b, caused by truncation during the transfer from k-space during the inverse Fourier transform of the output data. This occurred in the scanning process and is difficult to avoid, since it occurs in sharp shifts of intensity (Somasundaram and Kalavathi, 2012). They most clearly appear

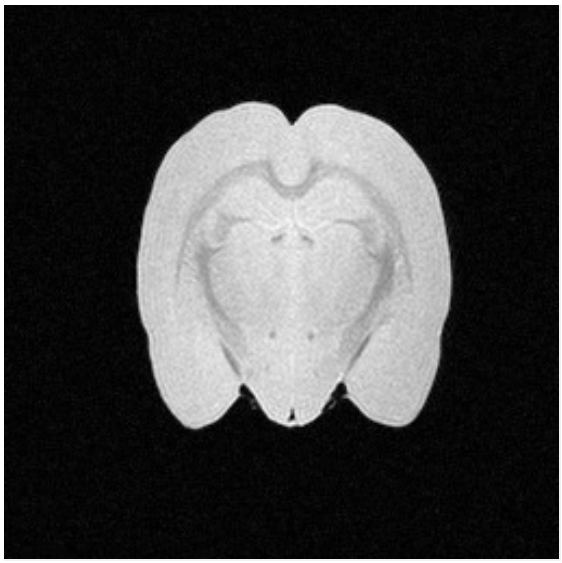

(a) Sham animal with different coil. Notice the grainy look present throughout the entire brain

(b) Animal displaying Gibbs Ringing, especially clear if you look close to the edge of the brain within the red box.

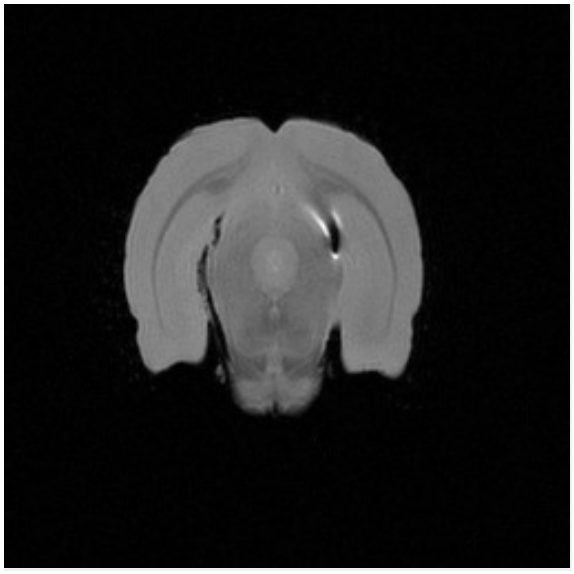

(c) One of the discovered holes.

Figure 4.2: Abnormalities that were found when analysing the images.

as thin lines next to these shifts, and they are visible close to the edge of the brain, since the major shift in intensity between the fomblin around the brain and the brain itself. It is however unlikely that it has affected the results of this report, since the focus is placed on the corpus callosum, which is located further inside the brain. The shift in CC, between gray and white matter, is much lower than that between brain matter and fomblin. These artifacts mentioned above were not amended for, except for the choice to discard the sham animal with a coil different from the other animals. This was done since variations in how the images are recorded could lead

to small changes in the measured results and the injuries that were examined are small. The holes could be disregarded since they are outside the CC, which is the region that was examined in this thesis.

4.4 Region detection and extraction of corpus callosum

When detecting the CC using the method described in section 3.4, the intermediate result is the traced line that will likely trace within or alongside the edge of corpus callosum. One such line is shown in figure 4.3. This line is traced along the b0 image of one of the normal animals.

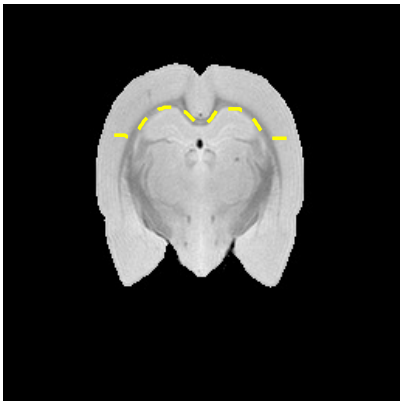

Figure 4.3: Line traced alongside the CC of the b0 image of an normal animal.

After the parameters for detecting the line had been customized for the data, the selection around this line was made. Visual inspection showed that the resulting mask was mostly limited to the CC and the regions just around it, see figure 4.4. Figure 4.3 displays the line that was used to create the mask that is shown in figure 4.4 as a region with increased intensity.

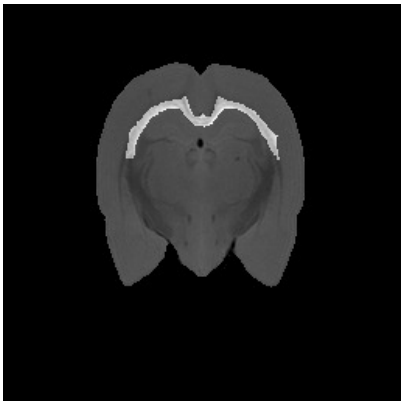

Figure 4.4: The area with increased brightness is the area covered by the detected mask.

The mask itself is a binary volume that can be used to extract values belonging to the CC. It can be viewed in a 3D view to watch the outline of the area masked. This is shown in figure 4.5.

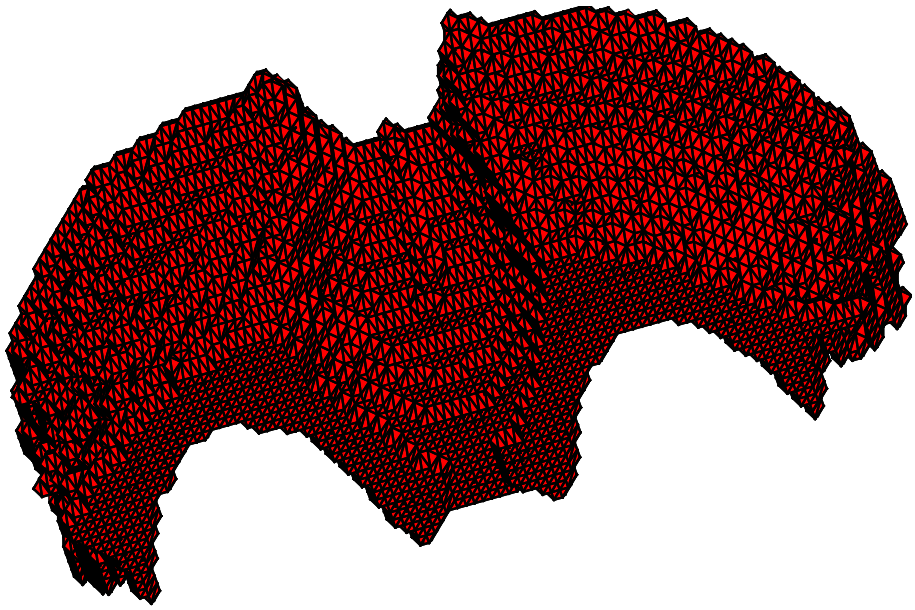

Figure 4.5: 3D view of the resulting mask, for a selection of slices.

4.5 Evaluation of techniques for processing data

The following sections will display results both from literature but also findings from analyzing the data. Fractional anisotropy, tractography and computing the mean values of the whole brain is studied.

4.5.1 Evaluation of fractional anisotropy

Fractional Anisotropy as an evaluational tool offers some strengths, but also has some weaknesses. It is important to be aware of these when analysing results and images in order to be able to draw conclusions, and as such these will be presented here. The equation for FA was shown in equation 1.2. The equation is created in a way such that if the eigenvalues increase or decrease by an equal amount, the resulting FA value will remain unchanged. If the evaluation for injuries was limited to solely examining the FA, it is possible that regions that changed diffusion coefficients quite drastically would go entirely unnoticed.
This theory was evaluated when one exposed animal was examined, the effect of this shown in figure 4.6. It is seen here that the left side of the corpus callosum displays elevated eigenvalues compared to the right side, in λ_{1-3}. The lower eigenvalues typically have values that allow the CC to be easily distinguished from the gray matter surrounding it. The FA map however does not indicate that there is any major difference between the right and left sides of the CC. It is likely due to all of the eigenvalues shifting a similar amount in the left side of the CC, which is likely

caused by an injury, but not by an axonal injury. Without a histological examination it is difficult to be certain, but it has the appeareance of a collection of fluid, making an edema a likely cause.

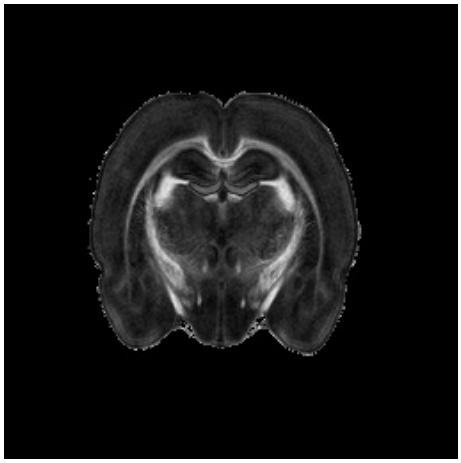

(a) FA map, note how there is no clear difference between each half of the CC, as is seen for the eigenvalues

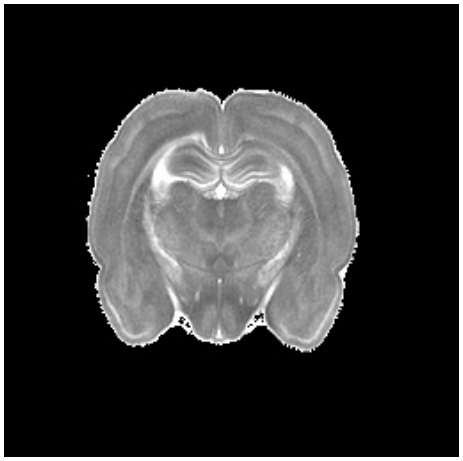

(b) λ_1, right half of the corpus callosum is clearly elevated when compared to other animals and the right half.

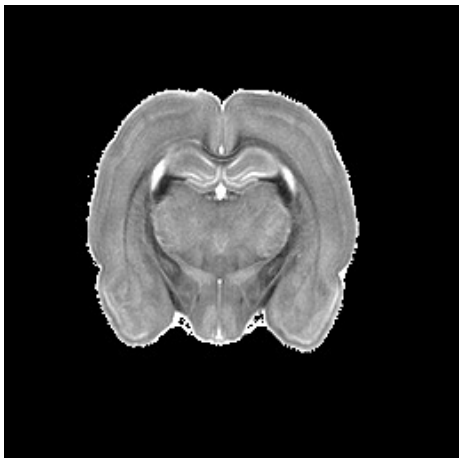

(c) λ_2, right half of the corpus callosum is clearly elevated when compared to other animals and the right half.

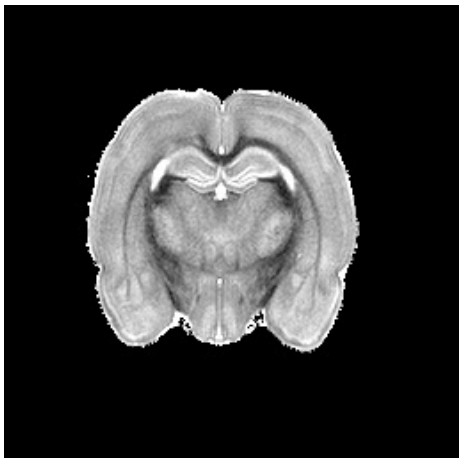

(d) λ_3, right half of the corpus callosum is clearly elevated when compared to other animals and the right half.

Figure 4.6: The images displays the same slice for the same animal, but for different parameters. Note how in the FA map both sides of the corpus callosum appear to be rather similar, as expected, but when examining the eigenvalues it is clear that the left side of the corpus callosum has elevated values when compared to the right side. Since all of the eigenvalues appear to have increased by similar amounts, the FA value is unchanged.

On the other hand one of the main strengths of FA is that it unaffected by how the brain is placed in the MRI. It does not matter if one brain is place at an angle

compared to another, since FA compares the amplitude of diffusion in the three principal directions of each voxel.

4.5.2 Evaluation of tractography

Tractography is based on the diffusion tensor with the corresponding fiber orientation. In this case there are 30 different values of diffusion and one reference b0. The algorithm mentioned in section 3.3 is reconstructed to a tensor matrix meaning that the 31 values becomes six values, the six different tensor elements. The eigenvalues and eigenvectors of the diffusion tensor are easily calculated afterwards. These eigenvalues are then used to extract the largest value of diffusion in each voxel and its orientation (the corresponding eigenvector), which can be taken as an approximation of the direction of an axon passing through the voxel.
The problem with this is the assumption made that the largest diffusion axis corresponds to the axons directions. There might be bundles of axons, multiple axons crossing each other in a voxel. The smallest face of each voxel is 0.11x0.07 mm^2. One myelinated axon has a mean diameter of 1.5 μm (Komlosh et al., 2013). This means that about 4350 axons could fit in a pixel if they were closely packed. The assumption then states that all of these axons are in the same direction, which most are, but not all. This is because the local architecture varies in the white matter and can contain a significant amount of complexity such as bundles of axons.
Another limitation with tractography is that it cannot detect synapses, fiber endings. This means that the fiber tracking ends when it reaches a voxel of low anisotropy (Jbabdi and Johansen-Berg, 2011), and since injuries might be present in areas with low FA, voxels that are relevant might be missed.
However, Tractography was still tested using DSI-studio (Yeh et al., 2013). The result is shown in figure 4.7 where the default values of DSI-studios were used for the stopping criterion of the tracts and the run was terminated at 25 000 tracts, the CC was marked as a region of interest and after allowing the whole brain for seeding tracts that passed through the region of interest were kept.
The tracts were colored of with the average direction of each tract. There are quite a lot of tracts passing through the corpus callosum, making it difficult to determine if differences between different tractographies are injuries or a result of differing sizes of the brains.

4.5.3 Evaluation of mean and standard deviation of the eigenvalues

A measure that can be compared without any spatial normalization is the whole-brain mean values and standard deviations. This was performed on the animals included in the study, and the result is shown in figure 4.8. As we can see in the figures 4.8b, 4.8c, 4.8d and 4.8a. The FA value and all eigenvalues do not appear to follow any clear trend, and the standard deviation makes it difficult to draw any clear conclusions from this method. The large standard deviation likely stems from the fact that by taking the mean and std values of the whole brain large quantities of both white and gray matter are included.

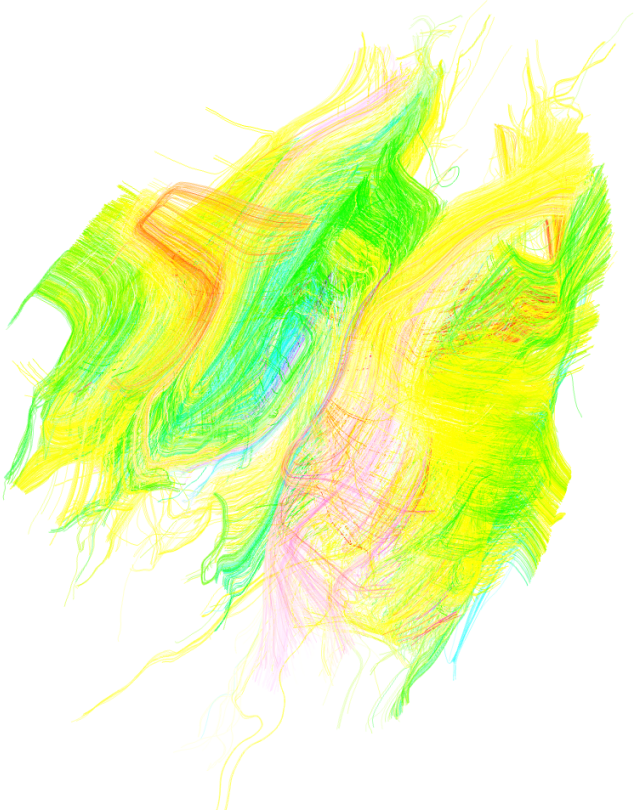

Figure 4.7: Tractography with 25 000 tracts going through CC, each tract is colored with the average direction within the tract.

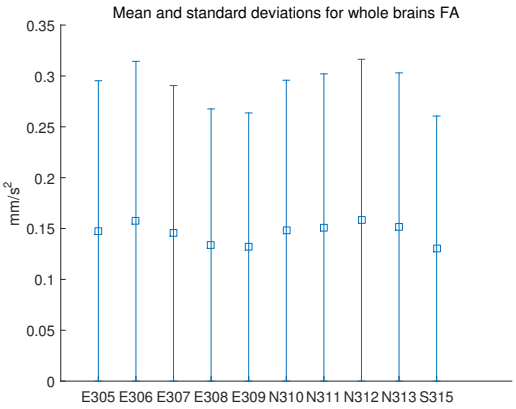

(a) Mean and standard deviation for FA.

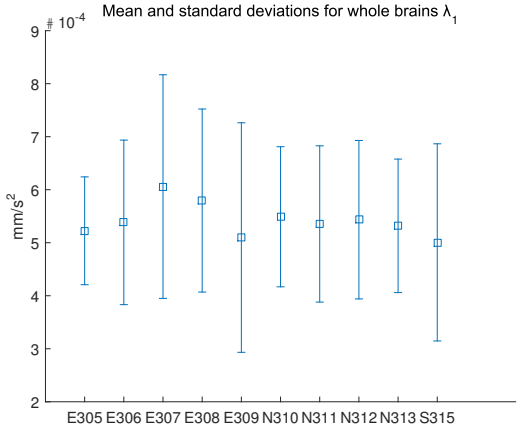

(b) Mean and standard deviation of λ_1.

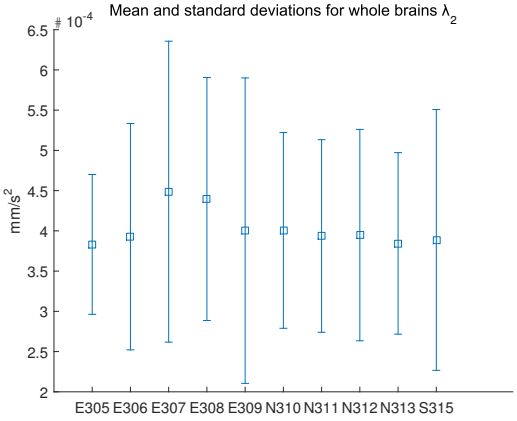

(c) Mean and standard deviation of λ_2.

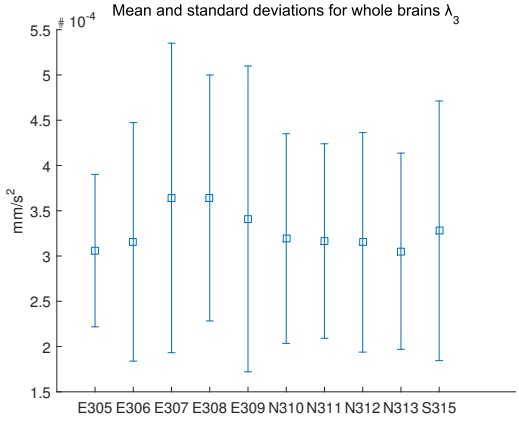

(d) Mean and standard deviation of λ_3.

Figure 4.8: Mean values and deviations of FA and all the eigenvalues. Since the std is so big compared to the mean value, these results cannot support any clear conclusions.

4.6 Spatial normalisation

In figure 4.9 the same slice for one brain is shown before and after affine translation, calculated by the method described in 3.6 on the b0 image. Green areas indicate that one animal had higher intensity than the other, purple areas indicate that the values of the second animal is greater than that of the first one. Areas in grayscale have approximately equal values prior and after the registration

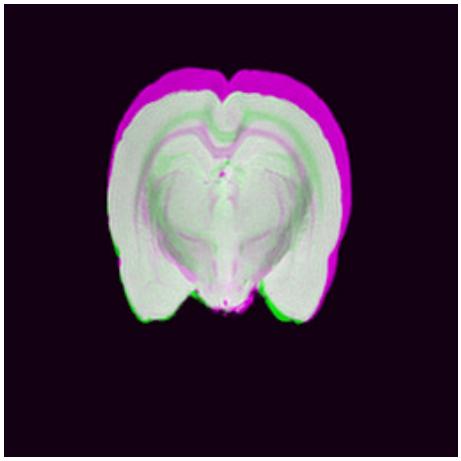

Figure 4.9: The same slice of one animal before and after affine registration placed in the same frame.

Displacement was carried out on the affinely aligned images and a comparison before and after the displacement is displayed in figure 4.10.

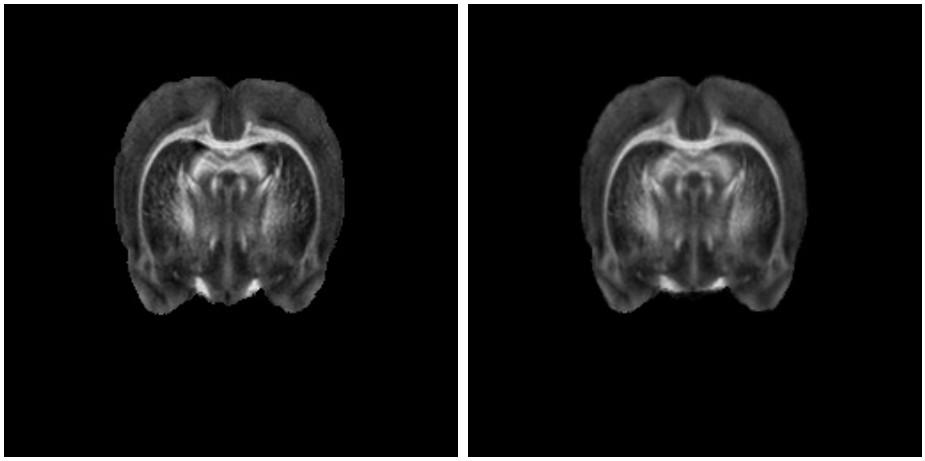

(a) FA value after the affine translation.

(b) FA value after applying a displacement field.

Figure 4.10: Image before and after applying a displacement field. Note how the CC shifts.

Due to the process of displacement, the resulting images are slightly blurred which makes comparisons between the target image and the spatially aligned images difficult. However, since all images are handled in the same way (except for the target), comparisons between different aligned images should be possible.

4.7 Voxel-wise analysis

After performing the registration as presented in previous section, the resulting images where examined as described in section 3.7. In figure 4.11 we can see the result for this procedure in one slice of the FA map for each of the animals. Voxels that are not close to the CC have been excluded. Should one wish to change the region of interest or include the entire brain it can simply be altered. There are three animals that have more marked voxels than the others: E308, E309 and S315.

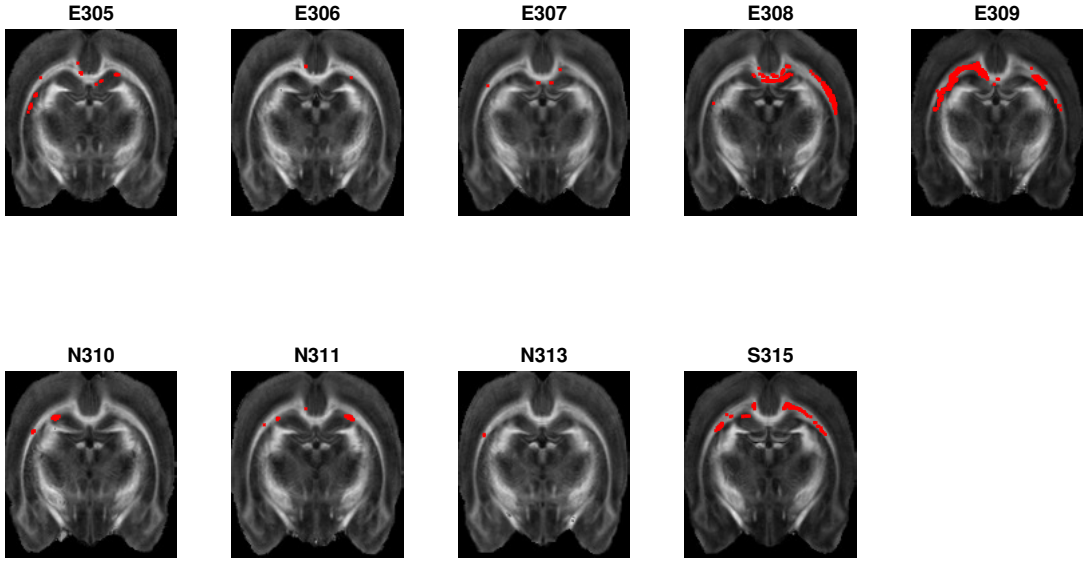

Figure 4.11: View around bregma -1.5 (slice 28) of the FA map for all aligned and deformed animals. Red marked voxels indicate that the value of this voxel are significantly lower than the mean value. Voxels that are not in or near the CC have been excluded.

The amount of voxels marked for each slice was also calculated and the obtained results are shown in figure 4.12.
There are three outliers that appear to have more voxels marked than the other animals throughout the entire CC. E309 was mentioned earlier as an animal where the FA value could be misleading, see section 4.5.1, which could have been caused by an edema, since a change in eigenvalues appeared to be clear in one area while the FA value was not as clearly changing. It appears from the result of the voxel-wise analysis as if the entire set of data from the animal E309 has a significantly lower FA value than the rest of the animals, causing a large amount of marked voxels throughout the brain. E308 on the other hand seems to have a slightly misshaped brain on one half, which is shown in figure 4.13. The figure displays the brain before and after the attempt to correct this defect.

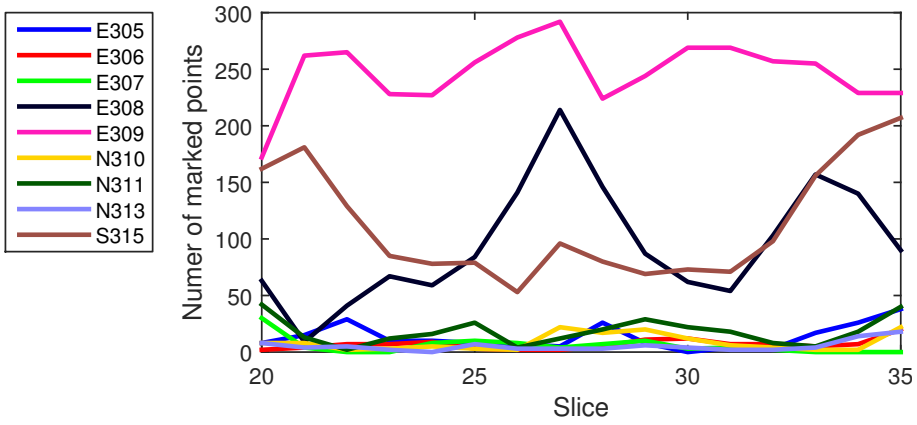

Figure 4.12: Amount of marked voxels for each the slice for all of the animals, spanning roughly over the entirety of the corpus callosum.

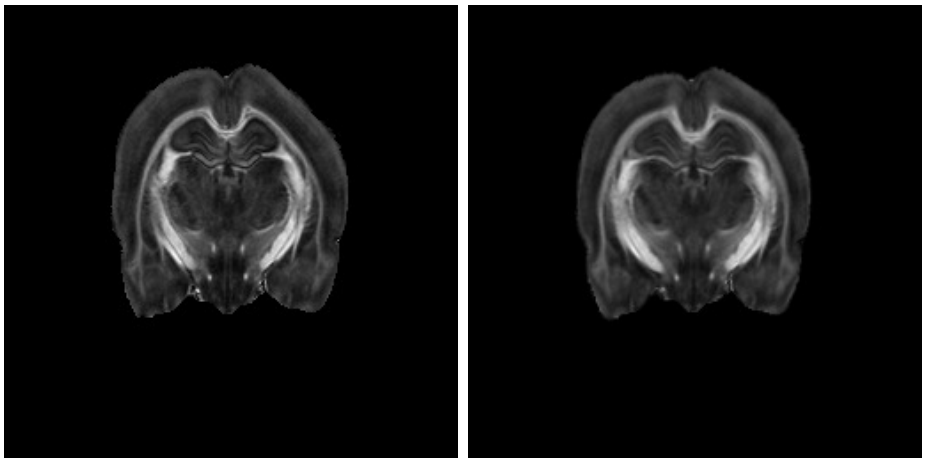

(a) FA value after the affine translation of E308.

(b) FA value after applying a displacement field to E308.

Figure 4.13: Image before and after applying a displacement field. Note how the corpus callosum shifts on the right side as the indentation of the brain is attempted to be corrected.

It appears as if this correction was not entirely successfully. This because the major part of all marked voxels is in this misshaped part of the brain and likely the cause of these voxels. The third animal that showed several marked voxels was S315, which was a sham animal.
Compared to the hypothesis postulated in the beginning of the methods chapter, this protocol is intended to detect singular voxels that differ greatly from surrounding tissue. As such it is not expected that there would be marked points throughout the entire CC for any of the animals, but hopefully there would have been slices where the exposed animals had clusters of injured voxels. The choice of using a difference of two standard deviations seems rational, since the outliers would be outside the 95th percentile, but using stricter comparisons (i.e. more standard deviations, such as three or four) would reduce the amount of marked voxels, and could be interesting

to look further into.
In order to improve the result, two additional sham animals from a different study were added as described in section 3.7. The resulting marked voxels in one slice are shown in figure 4.14 and the amount of marked voxels for each slice is shown in figure 4.15.

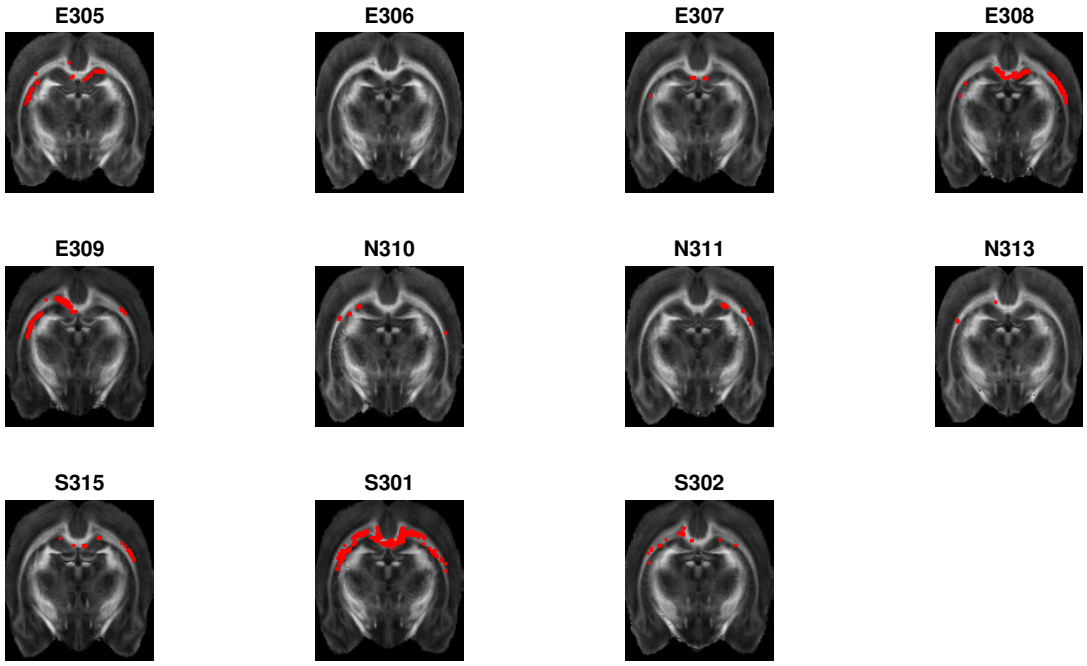

Figure 4.14: View around bregma -1.5 (slice 28) of the FA map for all aligned and deformed animals, where two additional healthy animals were added. Red marked voxels indicate that the value of this voxel are significantly lower than the mean value. Voxels that are not in or near the CC have been excluded.

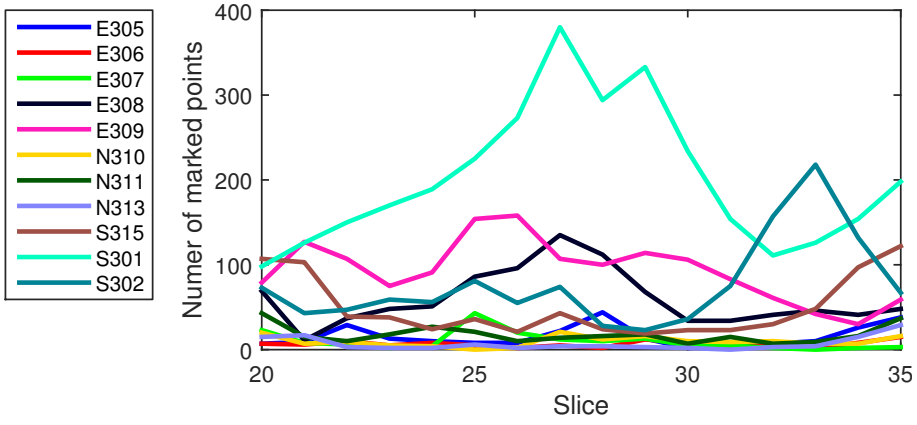

Figure 4.15: Amount of marked voxels for each slice for all of the animals with two additional healthy animals, spanning roughly over the entirety of the corpus callosum.

It appears as if the added animals had a average lower value then the original animals. This caused many voxels to become marked in these supposedly healthy

animals. S301 especially had a very large amount of marked voxels, but the addition of these two extra images significantly reduced the amount of voxels detected in the three outliers from figure 4.12.
In an further attempt to improve results, histogram matching was performed to normalize the amplitude of the image sets. This was performed as described in section 3.7. In figure 4.16 images of E309 with and without histogram matching applied prior to the displacement is shown.

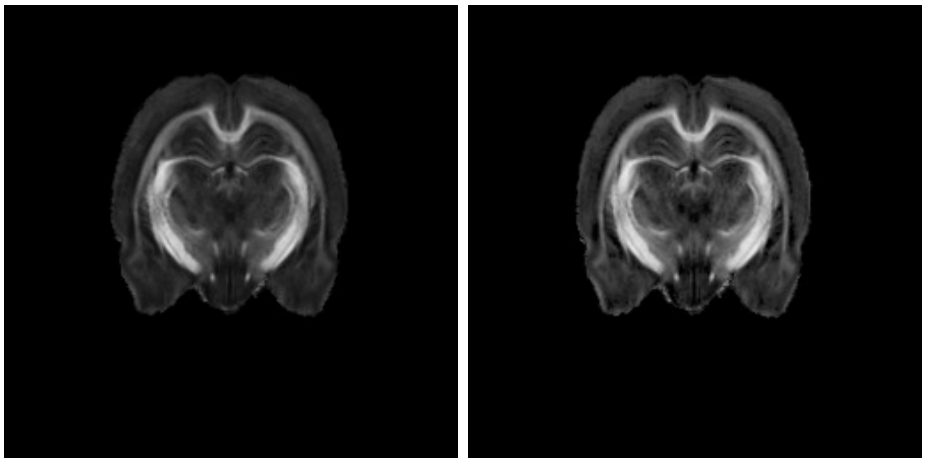

(a) FA value after displacement on E309, without histogram matching.

(b) FA value after displacement on E309, with histogram matching.

Figure 4.16: Result from displacement with and without applying histogram matching. The result in this case appears to be an overall higher FA value after matching, which seems reasonable since this volume had on average lower values prior to the histogram matching.

Histogram matching with the target (N312) was performed prior to deforming the image volumes, with the reasoning that since amplitude normalization makes the images more similar, the displacement field method should work even better. The same slice as previously displayed is shown again with marked voxels in figure 4.17 and in figure 4.18 the amount of marked voxels for each slice is shown.
After performing the histogram matching, the average amount of marked voxels for each slice dropped. The amount of marked voxels seems more even amongst the animals compared to when histogram matching was not used, as was shown in figure 4.15. The two added sham animals still appear to have a lot of marked points and might not pass as normal animals for this study. However, even without disregarding the added sham animals, the amount of voxels marked when comparing normal and exposed animals does not appear to be significant. While some exposed animals appear to have fairly high counts (especially, once again, E309 and E308), further investigation would be necessary to draw solid conclusions. One thing does appear to fairly clear: That for some reason the two added sham animals seems to differ in from the other animals, which goes against what was expected, since the procedure they underwent should not affect the CC.

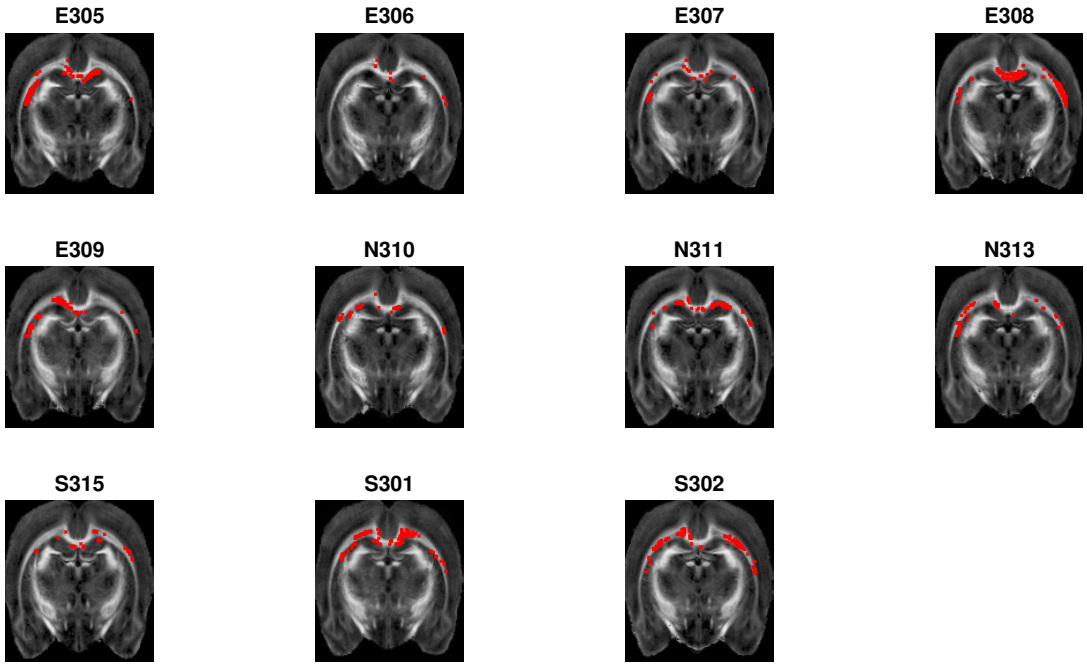

Figure 4.17: View around bregma -1.5 (slice 28) of the FA map for all aligned and deformed animals after performing histogram matching prior to displacement. Red marked voxels indicate that the value of this voxel are significantly lower than the mean value. Voxels that are not in or near the CC have been excluded.

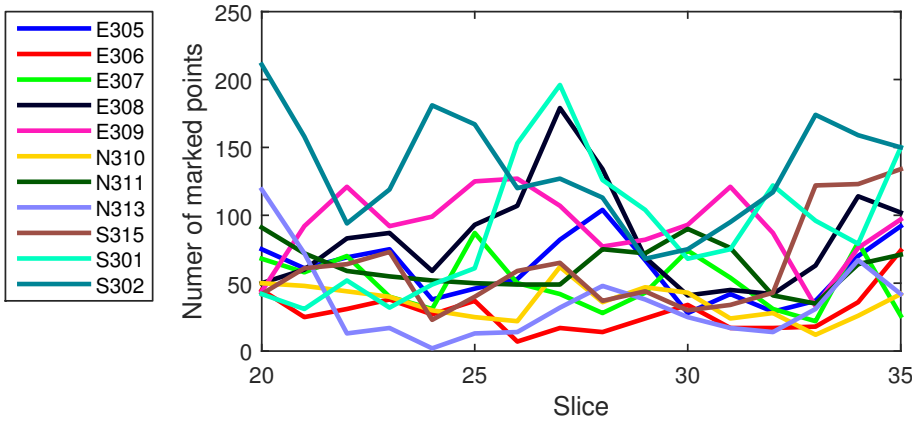

Figure 4.18: Amount of marked voxels for each slice for all of the animals with histogram matching prior to displacement, spanning roughly over the entirety of the corpus callosum.

4.8 Examining voxel values within corpus callosum

4.8.1 Examining trends within subjects

When comparing voxels within the CC for an animal in the midsagittal plane, the same pixel in adjacent slices do not correspond to each other as mentioned in section

3.8.1. This is because CC is slightly arced, as seen in figure 4.19. To be able to account for this arc between slices some equations were required. A rough estimate was done by taking two pixel along the CC and rewrite them on point–slope form, see equation 4.1 and 4.2. The result from this was that when comparing slices in the frontal plane the pixel needs to be compared with the pixel above or below when moving two slices forward or backwards. Then to be able to compare pixels within CC the mean of two pixels were computed and compared with one pixel from the previous slide.

$$\frac{\Delta x}{\Delta z} = \frac{(93-68)\cdot 0.07}{(33-20)\cdot 0.5} \approx 0.0728 \tag{4.1}$$

$$\arctan(0.0728) \approx 0.0727 \approx 4^\circ \tag{4.2}$$

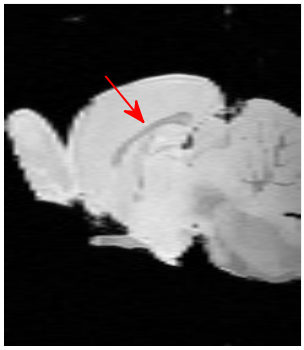

Figure 4.19: Rat brain viewed from a midsagittal plane, the red arrow is pointing on the CC.

4.8.2 Examining trends within all gradients

Cluster analysis was performed separately on the 30 gradient directions using all pixels within CC. This was to examine whether the allocation of the various diffusion values can be used to distinguish between values from the exposed and normal subjects. All subject were used in these tests and the focus was on one slice only, bregma -2.5 mm. The 30 directions were tested one by one to see if the subject values differ in weighted neuron, figure 4.20. Different sizes of the self-organizing maps were tested to examine how the distribution of the neurons would change, that is, how the color would change. The results of the various tests were similar and no result was clearly differentiable from another. Therefor no additional tests with this tool were made.

Proceeding from cluster analysis, changes in direction values were examined. By comparing the difference in directional value (values prior diffusion). This were performed by subtracting the mean value of two pixels with one pixel value of the previous slice of the frontal plane, that is using the equation 4.1. This because of the arc on CC mentioned in section 3.8.1 and previously in the results, section 4.8.1. The results that were produced are seen in figures 4.21a and 4.21b. The images display some white lines which are probably because the value of the following slide

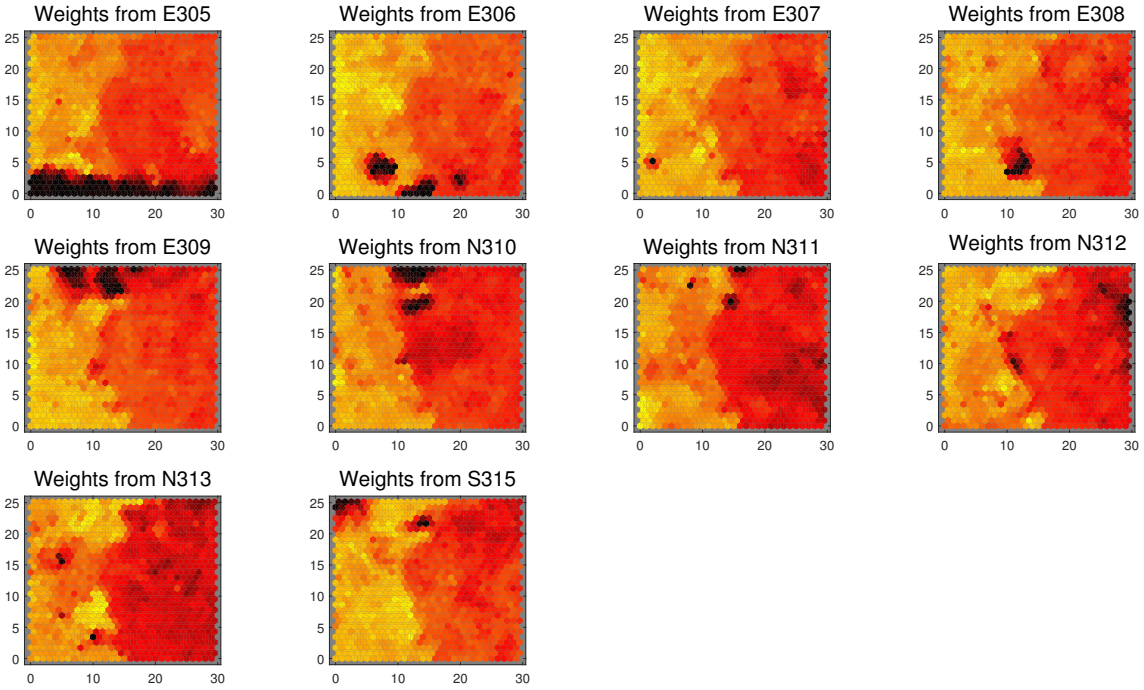

Figure 4.20: Neural networks clustering displaying the third diffusion direction for all subjects around bregma -2.5mm. The size of the two dimensional self-Organizing map is 30 which can be visualised on both axis. If there would have been a different distribution of neuron values the colors would have been changed both brighter and darker

were not inside the CC mask used. The three masks used were developed by hand. There is a pattern here that seems to be repetitive among the exposed animals which is the irregularity in the first two slices of the exposed animal compared to the normal animal. The values on the y-axis are not weighted diffusion but prior data, referred to as raw directional data or just directional data. The purpose of these plots is not to visually spot the differences but to study recurrent patterns from exposed animal that deviates from the normal animals. Therefor the data was not converted to diffusion.

Some amplitude differences were spotted when examining the raw directional data. This can be seen in figure in 4.22a. The figure displays the raw directional mean value for each slice inside CC, between bregma 2.5 and bregma -5.4 for all animals. There is a clear difference in levels between some animals. The same difference was also found in the b0-images, figure 4.22b. When taking the raw direction values and accounting for the b0-images to produce weighted diffusion values, the amplitude changed. See figure 4.25 compared to 4.22a. So comparison between raw directional data should not be done because it would be misrepresenting. The data used in figure 4.25 and figure 4.22a is the mean value of each slice.

The next step was to examine if the pattern seen in figure 4.21, of the different gradient directions, could be visible when examining mean and median values for each gradient direction of each animal. The tests were primarily done to reduce the size of the data sets. This reduction resulted in 18000 samples instead of the previous

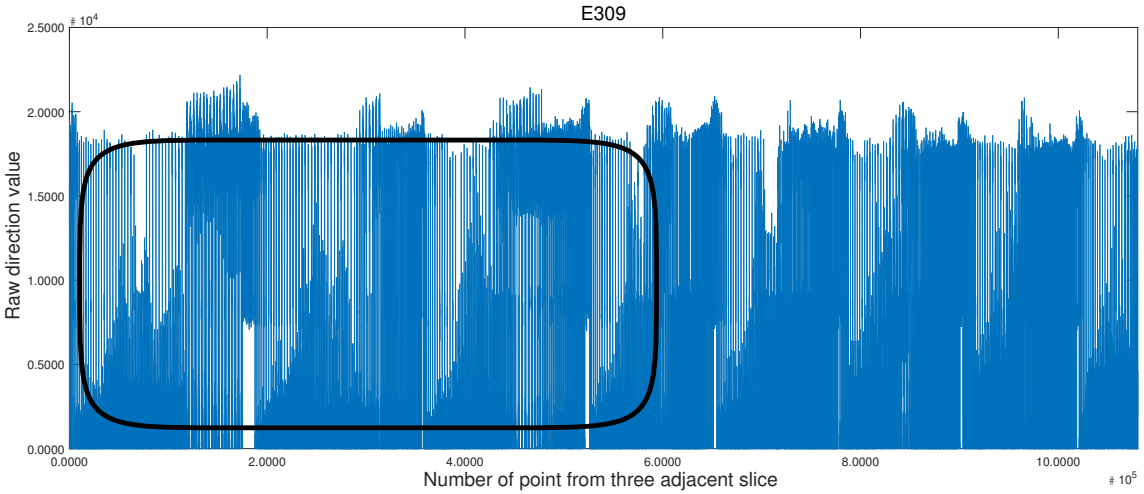

(a) Animal E309

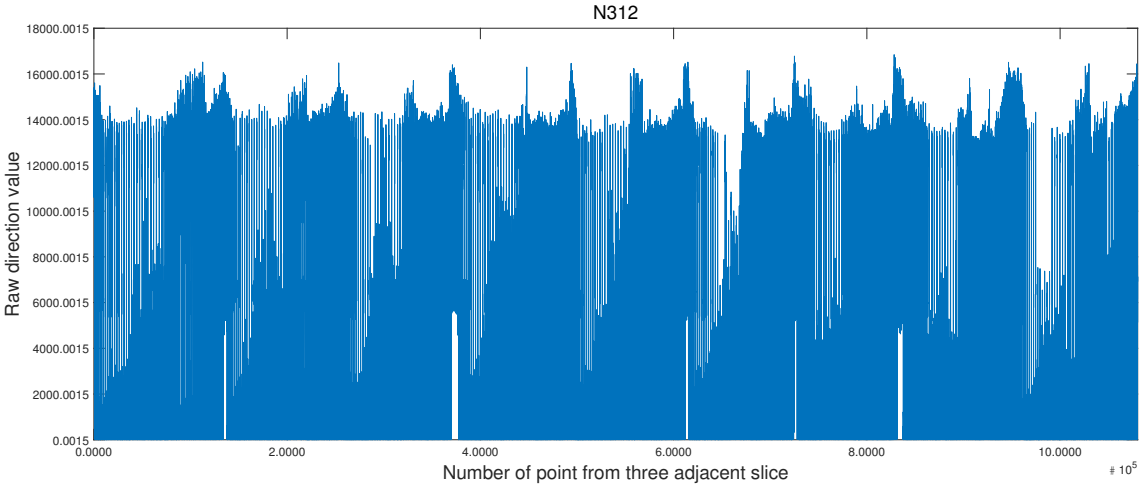

(b) Animal N312.

Figure 4.21: Voxel-wise changes between three consecutive slices, bregma -0.5mm to -1.5 mm, inside CC using hand made mask, taking into account that CC is slightly arced. The first half of the x-axis displaying differences between first and second slice and the second half differences between two and three

$12 \cdot 10^6$. The images used were not aligned and the mask was hand made focusing on values within corpus. This was done so that changes were due to injuries and not due to the amount of gray matter in the masks. The data has been converted to diffusion in order to compare them in the same plots. The data was first displayed as data plots displaying the mean values, figure 4.23. Followed by statistical analysis. Standard deviations of mean and median values for each animal were extracted, see table 4.2. The data plots are the mean of each direction for ten consecutive slices from bregma 1.5 mm to -3 mm. The results were quite promising when comparing normal to exposed animals, therefore more tests using mean and median values were performed. The mean values of all animals are displayed together in figure 4.24. For more plots containing all animals separately (other than those two already presented

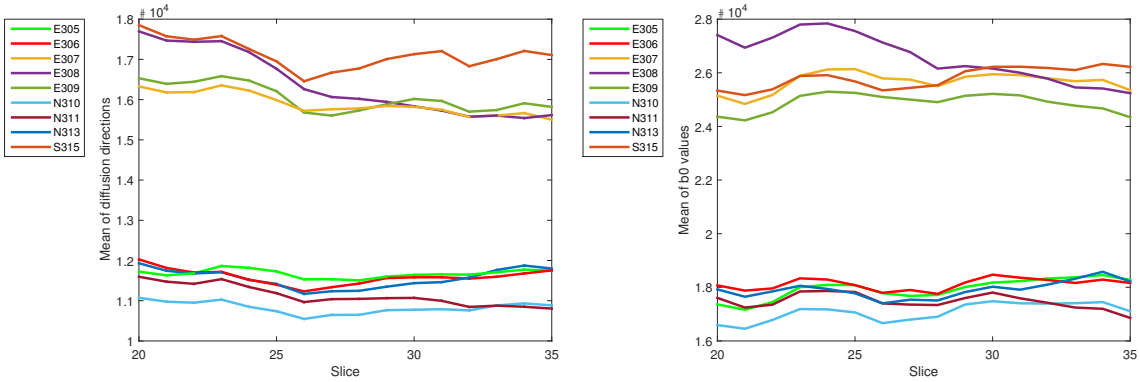

(a) Mean value of the raw direction values for each slice.

(b) Mean value of the raw b0 images for each slice.

Figure 4.22: The images are displaying slices from 20 to 35 which corresponds to about +2.52 mm to -5,4 mm from bregma. All nine subject with 30 gradient directions has been used and registered to N312.

here) see appendix A. When displayed together its difficult to tell the animals apart. Mostly since the data from the sham animal exhibits a higher amplitude then the rest. To proceed with this result more analysis were used covering bigger part of CC, calculating diffusion for each direction and FA values.

Table 4.2: Extracted STD of mean and median values from data in 4.24, all animals, It displays the mean STD of all slices included in the analysis

STD of median values					
Normal	8.746e-05	8.24e-05	8.411e-05	8.477e-05	7.536e-05
Exposed	7.907e-05	8.643e-05	6.721e-05	6.593e-05	5.327e-05
STD of mean values					
Normal	8.484e-05	7.473e-05	8.841e-05	8.164e-05	10.64e-05
Exposed	6.889e-05	9.372e-05	7.284e-05	6.593e-05	8.385e-05

The table 4.2 lists some differences in std between normal and exposed. However, the std for each slice from normal and exposed were not found to be different. When trying to plot just the std for each slice the result did not show any differences between normal and exposed.
When the raw direction images from normal and exposed animals were evaluate the mean value in each slice from slice 20 to slice 30, it was noted that the data had similar amplitude differences, see 4.23. The correction of these amplitude differences can be seen in figure 4.25. The same data was used in the classification method in section 4.9.
Another method that was tested was calculating the mean and std values of FA. This was performed for all pixels within the CC in each slice using the FA values. This was performed on the images that were affinely registered, and the result is shown in figures 4.26 and 4.27.
In comparison to these images (figures 4.26 and 4.27) the result after full normalization can be compared: In figures 4.28 and 4.29 the results after displacement of

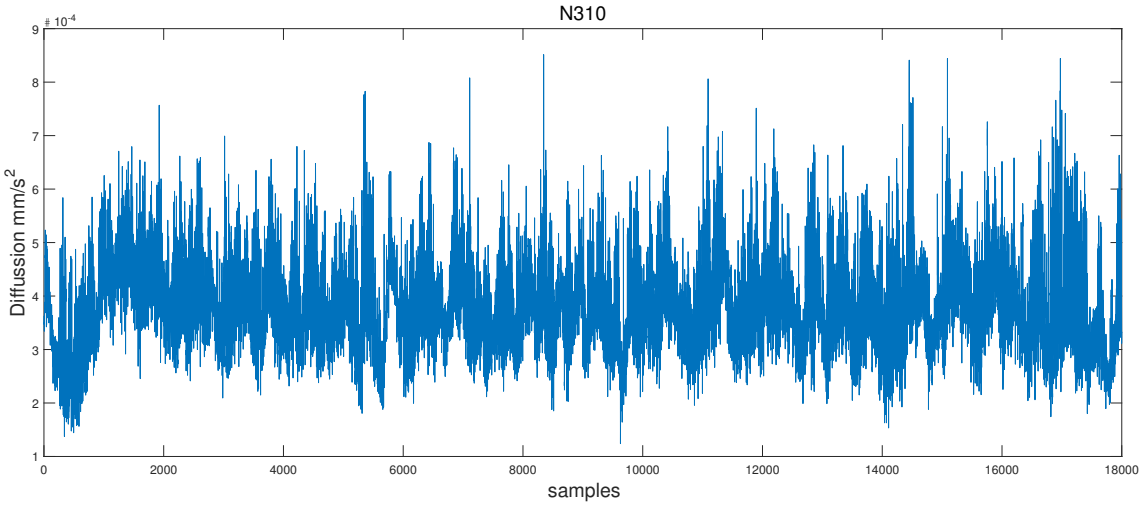

(a) Animal N310

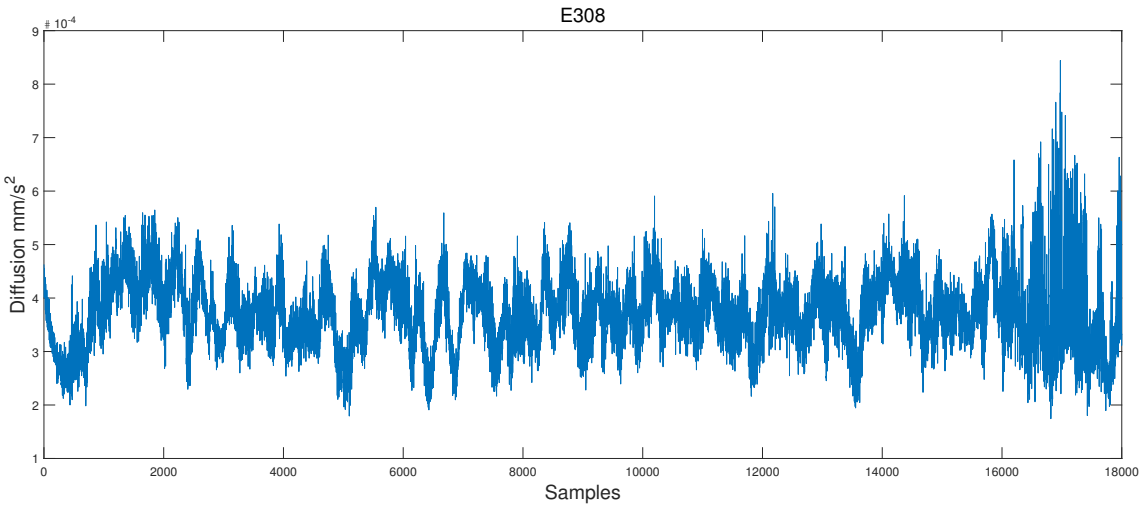

(b) Animal E308

Figure 4.23: The plots displays one normal and one exposed animal, this was done on all animals and the result were similar to this. The exposed animal had lower range of diffusion in most of the cases but not in all.

histogram matched values. It is clear that the spread of both the mean and std values were reduced. This is interesting when the issue of over alignment is considered. Over alignment meaning erasing different distinctions between the images. It is difficult to say exactly when this occurs and indeed this might be the case here.

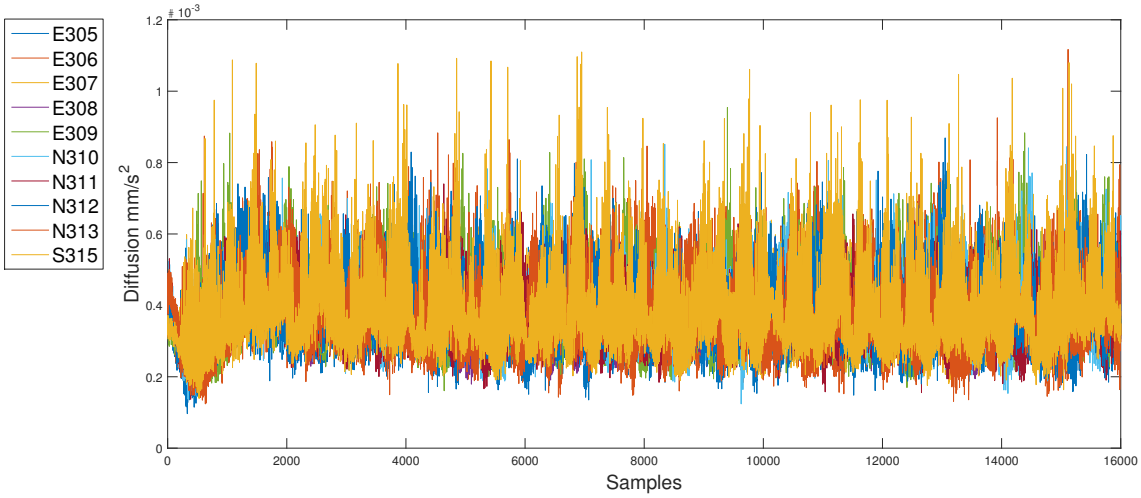

Figure 4.24: The mean diffusion value from ten consecutive slices from all animals

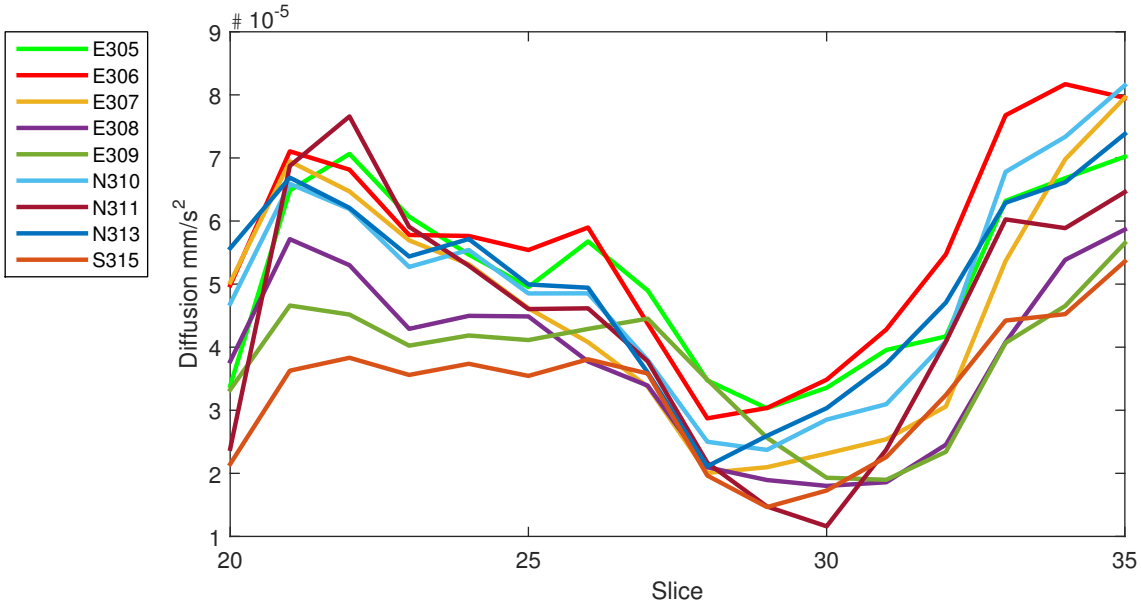

Figure 4.25: Mean diffusion for all gradients per slice, from ten slices, bregma +2.5 to -5.4, for all animals

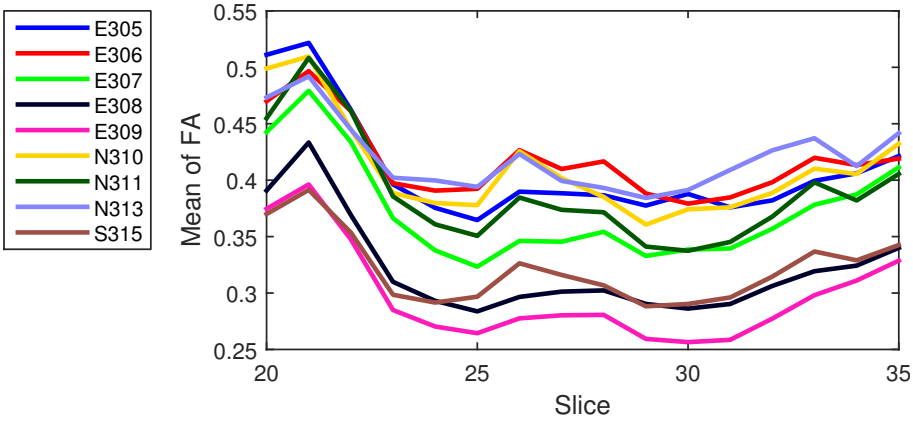

Figure 4.26: Mean value of the FA value for each slice using the mask created by hand on the affinely aligned images.

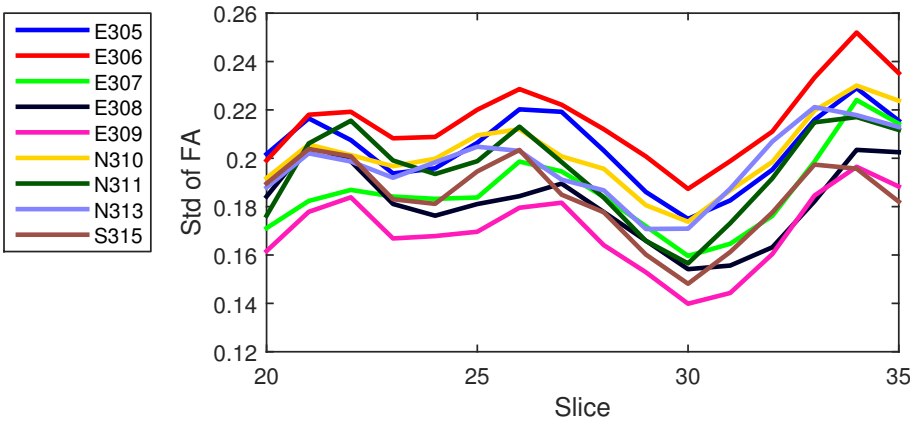

Figure 4.27: Standard deviation of the FA value for each slice using the mask created by hand on the affinely aligned images.

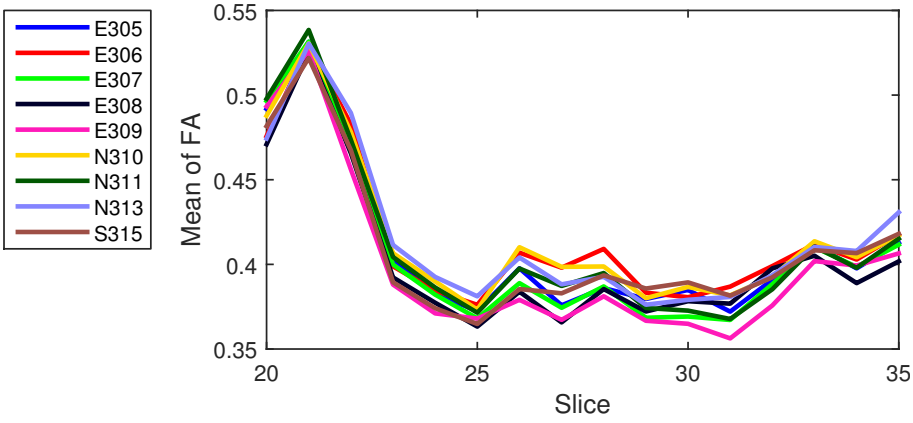

Figure 4.28: Mean value of the FA value for each slice using the mask created by hand on the fully normalized images.

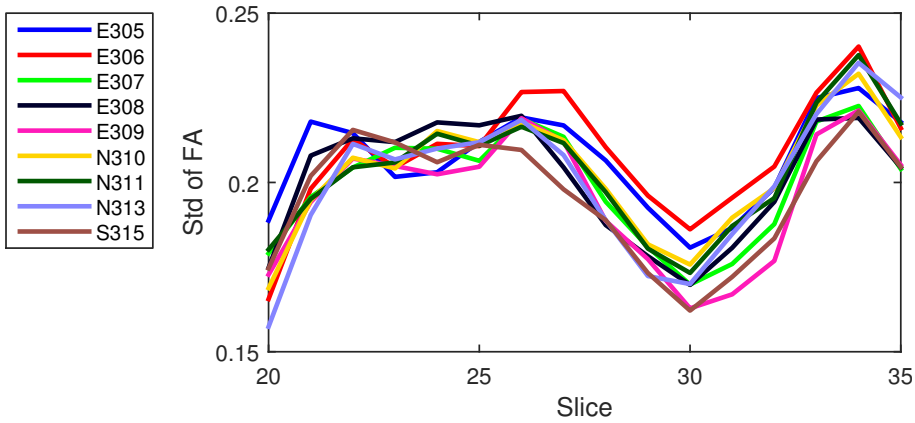

Figure 4.29: Standard deviation of the FA value for each slice using the mask created by hand on the fully normalized images.

4.9 Categorization of exposed animals using classification

The results from the discriminant analysis and the neural network classifications that were used are displayed in table 4.3 and figure 4.30. The first row of the different matrices displays exposed animals and the second one normal and the sham put together. Both classifiers were tested ten times each to see if the method provided were dependent on the different training sets, since the data sets are randomly split up into training and test groups. The discriminant analysis classifier showed a stable 62.5 % accurate classification. The neural network classification, however, generally showed a higher percentage of accurate classification result, but was not as stable as the discriminant analysis classifier.
This was because it changes it's neurons for each training, and there is some randomness during the initialization. The Test Confusion matrix, displayed in figure 4.30, shows one outcome, that had a 100% accurate classification, which is excellent. The result is dependant on the training and both only occur when the training confusion matrix is a 100% accurate. The classification was tested on different data FA, the eigenvalues and the 30 gradient images. All were tested with the whole images and with just CC and some surrounding tissue. The 30 gradient mean value data gave the best classification result and were therefor displayed. The FA-values had a poor result, most over 66% miss classifications. The case displayed in figure 4.31 classes all as normal animals, and is as such unusable for classification.

Table 4.3: Confusion matrix using discriminant analysis classifier. The rows are actual class and the columns show predicted class.

	Exposed	Normal
Exposed	**5**	0
Normal	3	**0**

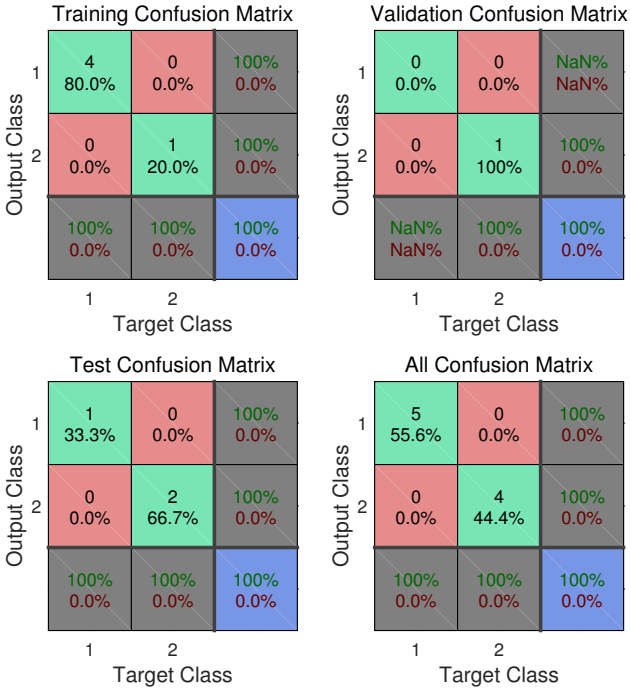

Figure 4.30: Confusion matrices displaying results from all the different steps in testing the neural network. The data used were the mean diffusion values per slices, figure 4.25.

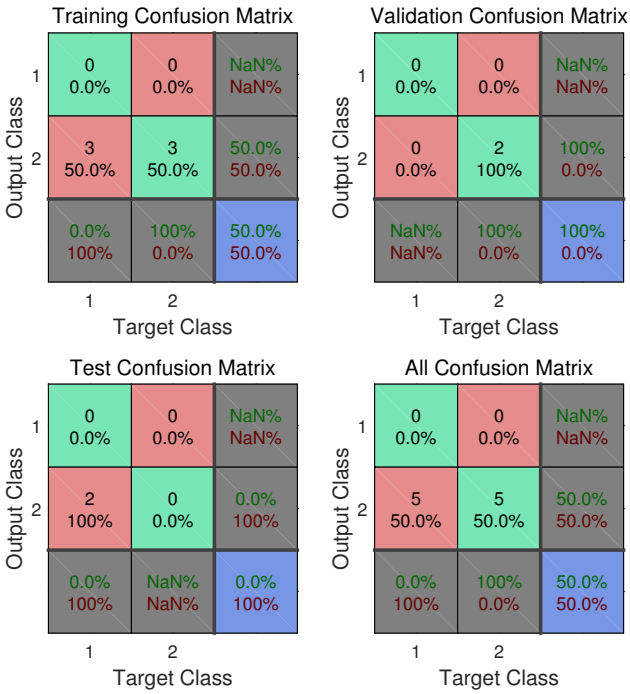

Figure 4.31: Confusion matrices displaying results from all the different steps in testing the neural network. The data used in this test were FA values that were fully normalized images.

5
Discussion

This thesis aims at developing a protocol for detection of axonal injuries using DT-MRI data. For this thesis DT-MRI data from animals that have been subjected to rotational head trauma, known to produce diffuse axonal injuries in several brain regions, were made available for analyses. Several types of analyses have been carried out as there were several elements that needed to be considered when moving forward with the analyses. The most important characteristics of the data is the fact that the axons are so many magnitudes smaller than the resolution of the DT-MR images. This was not the only difficulty encountered during this thesis and hence the choice of methods and how these choices influenced the results will be discussed here. First, work that was done prior to this thesis will be presented, then the work carried out in this thesis, and finally suggestions for the future will be conveyed.

5.1 Conclusions drawn from them analysis of work done by Carcedo

The results and conclusions provided by Carcedo is biased since the data analyzed were obtained by choosing a distance from what appears to be bregma and drawing conclusions about individual voxels, which allows for mismatch between the animals, which could lead to comparing white matter with gray matter. The mean value analysis on the other hand was fairly rough, the areas that means were taken over was fairly large, and the results (shown in table 2.2) show very small differences between normal and exposed animals, perhaps refining these areas into even smaller segments could have produced better results.
The amplitude normalization method adopted by Carcedo using eigenvalues from brain volumes including only gray matter and that were deemed uninjured could be useful, but first the consideration of whether or not normalizing using gray matter is appropriate when studying white matter. Our analysis provided that amplitude normalization could be done on a larger scale using histogram matching, which should be superior.

5.2 Usage of fractional anisotropy and tractography

Tractography has been suggested to be a useful tool to detect axonal injury in the injured brain. The main challenges using tractography to identify axonal injuries in

the CC stem from the fact that the corpus callosum is a relatively large brain structure, which contains thousands of axons. When these tractographies are generated the fractional anisotropy values are often are used to define the so called stopping point. The fractional anisotropy values are often used in combination with a limit on the angle of turning allowed for the established fibres. Injured axons in the relatively mild traumatic brain injuries studied in this thesis requires an extraordinary resolution to accurately follow the axons. Hence, the method does not lend itself to the detection of few axonal injuries and it is also uncertain that tractogrpahy can correctly describe a healthy animal.
There are other reconstruction methods that may be superior to traditional tractography. These methods adress the underlying difficulty with tractogrpahy, resolving more than one fiber orientation in a voxel, Farquharson et al. (2013), by the use of a technique reffered to as constrained spherical deconvolution. This technique appears promising, since it manages to detect changes along tracts that DTI was unable to detect (Auriat et al., 2015).
In this study the FA map of a particular animal did not indicate any deviation from the average animal although there was a clear change in all of the relevant eigenvalues on one side of the CC (4.6). The eigenvalues clearly indicate the presence of an injury, possibly an edema, in the particular animal. Despite this observation FA can still be a valuable too to detect injuries since it provides an easy way to understand regional white matter structure shapes. The calculation of FA values inherently normalizes the data values range from zero to one, and thereby simplifies the analysis and allows for convenient visualization of the DT-MRI data. However, using FA to detect axonal injuries appears to be difficult as the resolution in the state of the art DT-MR images are low; for FA to be a useful tool used to detect axonal injuries major improvements in image resolution are required.

5.3 Distinguishing normal and exposed animals

Differences between normal, sham and exposed should be determined using statistical methods. To enable such an analysis several tests were done on the animals. The results from these tests varies a great deal. Trying to find distribution deviations in hidden patterns or groupings between the exposed animal showed little success, seen in section 4.8.2. The same applies to the discriminant analysis classifier using FA, in section 4.9. The reason why FA showed poor result could be that information was lost when FA were calculated. It could also be because of the data used in the classification test, section 4.9, were the fully normalized images. These images could be over aligned, also known as overfitting. That is when the data is aligned to the point where originally distinguishing features are lost due to smoothing during the application of the displacement field.
The discriminant analysis classifier gave inferior results compared to the neural network. In this analysis different types of algorithms are used; the neural network that was used in this thesis is more advanced than the the discriminant analysis classifier. It is more advanced when creating the neurons that are fitted to each data set and adjust when all inputs and targets are presented. Discriminant analysis classifier does not adjust its values in the same way, it fits each group to a

covariance matrix. This suggests that either the difference between exposed and normal (including sham) animals data is very small or that the exposed animals injury is not located in the same region or that the exposed animals are not injured at all. However the neural network results suggest that there is a difference between the groups of animals that is sufficient to tell them apart. This suggests there is existence of injuries in the exposed animal and a pattern in locations of injuries of the exposed animals, since it is able to correctly classify the few animals that are left for testing after training.
The findings in the section 4.8.2 analysis of the mean of each diffusion directions suggest that there are some differences between the DT-MRI data of the exposed animals and normal animals(including sham). There was enough difference in the data for the neural-network to be able to separate the two groups of animals. However the classification analysis is not proven to be statistically significant since the number of animals are limited in this thesis. The separation between the animal groups were also successfully for the mean diffusion value for each slice even if the visual differences were minimal, see figure 4.25. However the overall mean for the whole brain, see figure 4.8 were data are similar and the std high. This suggests that the variations are confined to ROI and that was examined in this thesis, the CC. The differences appear to be regional and thereby difficult to pinpoint to individual voxels.

5.4 Normalization

This thesis identifies that normalization is a technique that appears to improve the image processing quality. In this thesis focus was on comparing scalar values, such as FA, while others have attempted to make registration methods that use multiple inputs (Park et al., 2003) (Zhang et al., 2006). These methods show interesting results, but were not realized in this thesis, because of the risk of overfitting. Even so, an interesting thing to consider is whether or not the addition of directionality (i.e. the eigenvectors) as an inputfor the spatial normalization would have contributed to the findings in a significant way. This consideration is highly important, if one should attempt to perform a tractography on deformed images, since that is not possible without directional information. Another option for the spatial normalization of the images could be to register each gradient direction individually and afterwards perform the DTI reconstruction as usual, which should, theoretically, produce images that are spatially aligned for all parameters. The method used here would have to be modified to perform such a normalization, but it could be a way to improve the results and could be worth looking into. Given the time it currently takes to register one brain (approximately 2-3 hours), this would increase manifold, which could make it difficult to use clinically where time is vital for treatment. It could however be interesting when performing studies on injuries and treatment methods where time is not as stressful, and since it is all done on the data processing end, it would not affect measurement times. Another thing to consider when heavily aligning images such as with the displacement fields applied in this thesis is over alignment of the images with the target, erasing differences that where present before the normalization. Developing metrics for determining whether the normalization

is a good fit, a bad fit or even too good of a fit would be useful when determining the success of the spatial normalization.
Amplitude normalization is another thing to consider: is the histogram matching carried out here a relevant method, or could it be further improved by matching the amplitude of a selected region, such as the normalization that was carried out by Carcedo? The histogram matching attempts to match the histogram of two entire data sets which should adjust for global differences in intensity. The normalization performed by Carcedo has one main weakness: is it always true that the chosen area is uninjured? Without performing additional studies of the region under microscope this would be difficult to verify.

5.5 Future Work

Our study suggests that spatial normalization of the image volumes could be improved by the introduction of multiple input displacement sequences based on all of the gradient directions before image registration could possibly produce even more reliable results.
The analysis clearly indicate that the most obvious way to facilitate an analysis that is targeted at dectection of axonal injuries using MR-DT images are an improvement of the resolution of the base images. The resolution of the images handled in this project is fairly large when compared to average axons, as mentioned earlier. If the resolution of the images could be improved by reducing the voxel size by around 4 times, the results from these methods could potentially increase greatly, by being able to visualize much smaller clusters of axons in each individual voxels, individual injuries could possibly be located. However, the issue with increasing the resolution without any underlying technical improvements is a decrease in the signal to noise ratio, which could cause injury to be hidden under noise. As such finding a proper level of resolution that allows distinguishing small injured regions without obscuring relevant data with noise is a difficult balance to strike.
Moving on from DT-MRI and using newer methods for recreating images is one way, but it places higher demands on the data sets, such as either increased gradient weighting for Q-Ball imaging or an increased amount of gradient directions for constrained spherical deconvolution (Tournier et al., 2008). These methods have shown promise in regions where fibers cross, and are likely useful for examining such regions.
Another way to continue with the tools available is to perform more measurements with the same measurement protocol on more rats, since that would supply a good statistical basis for continuing to evaluate neural networks and machine leanings ability to classify exposed and control animals correctly. This could possibly be combined with including injuries of other types and adding more classes to the classifier. The result from a test with classifiers such as this is not a display of where there is an injury, but rather a simple yes or no answer that says if a brain is injured or not. This has the benefit of being independent of human interpretation, but does not provide information regarding exactly where the injury is located.
Another way to verify that DT-MRI can successfully display injuries could be to create phantoms for validation: A collection of microscopic plastic tubes filled with

water could simulate axons, and by packing these close together you could simulate uninjured white matter. By then damaging some of these tubes in a controlled way, say by severing a portion of them, you could simulate a broken axon bundle. Indeed, phantoms such as this have been created by Tournier et al. (2008) for verification of the ability to resolve crossing fibres, but could possibly be used for verifying the ability to resolve injuries as well. An alternative to using phantoms could be the possibility of first taking images of live and healthy rats and then subjecting them to the trauma, followed by another set of imaging. This does present another set of difficulties, namely that of subject motion and breathing during imaging, which can create artifacts that are not present with the current setup.

6
Conclusion

Several different methods for detection of injuries have been attempted, with classification being the most promising one. None of them have provided entirely satisfactory results, but most of them offer options for going forward. Spatial normalization needs to be evaluated in order to determine whether or not the normalization method aligns the images too much. That is, removing the differences present in the datasets by aligning the images too much, smoothing out differences between animals. Classification shows promise, and could be a way to allow for distinction between healthy and injured brains. Performing a larger study to evaluate performance when using more sets of brains could be interesting and provide a way forward. Otherwise a study using phantoms as described in the discussion, section 5.5, could evaluate different reconstruction methods and compare their ability to detect injuries. To evaluate different reconstruction algorithms would require higher demands on the imaging protocol used. Demands such as increasing the amount of gradient directions used, to perform reconstruction such as Q-ball imaging or increasing the gradient weighting to perform high angular resolution diffusion imaging reconstruction. These methods are more focused on validating images and presenting a visible result, whereas classification forgoes the images and presents a simple yes/no whether or not the brain is injured. If it is possible to improve the resolution greatly and use voxel-wise analysis, this could allow for showing exactly where an injury is located rather than verifying whether there is one at all, which is valuable in itself. Classification would on the other hand provide a result that is completely independent from the operators interpretation.
So, to conclude, there are several ways to go forward with DT-MRI processing with the goal of detecting axonal injury: Either further focus on classification, phantoms for verification of the resolving power or improving the underlying imaging protocol to create images with an increased resolution are all interesting and valid topics to pursue further. Right now classification seems like the most promising tool for detection of axonal injuries using DT-MRI.

7

Bibliography

Adams, J. H., Jennett, B., Murray, L. S., Teasdale, G. M., Gennarelli, T. A., and Graham, D. I. (2011). Neuropathological findings in disabled survivors of a head injury. *Journal of neurotrauma*, 28(5):701–709.

American Association of Neurological Surgeons (2011). Patient information: Traumatic brain injury. `http://www.aans.org/patient%20information/conditions%20and%20treatments/concussion.aspx`. Online, accessed 2015-01-22.

Auriat, A., Borich, M., Snow, N., Wadden, K., and Boyd, L. (2015). Comparing a diffusion tensor and non-tensor approach to white matter fiber tractography in chronic stroke. *NeuroImage: Clinical*, 7(0):771 – 781.

Bazley, F., Pourmorteza, A., Gupta, S., Pashai, N., Kerr, C., All, A. H., et al. (2012). Dti for assessing axonal integrity after contusive spinal cord injury and transplantation of oligodendrocyte progenitor cells. In *Engineering in Medicine and Biology Society (EMBC), 2012 Annual International Conference of the IEEE*, pages 82–85. IEEE.

Beale, M. H., Hagan, M. T., and Demuth, H. B. (2015). Neural network toolbox™ user's guide. `https://www.mathworks.com/help/pdf_doc/nnet/nnet_ug.pdf`. Online, accessed 2015-04-27.

Benveniste, H. and Blackband, S. (2002). {MR} microscopy and high resolution small animal mri: applications in neuroscience research. *Progress in Neurobiology*, 67(5):393 – 420.

Boston College (2015). Physical constants. `http://www.bc.edu/schools/cas/chemistry/gradst/constants.html`. Online, accessed 2015-06-25.

Carcedo, M. G. (2012). Dt-mri image processing of animals brains with diffuse injuries.

Centers for Disease Control and Prevention (2015). Traumatic brain injury in the united states: Fact sheet. `http://www.cdc.gov/traumaticbraininjury/get_the_facts.html`. Online, accessed 2015-01-22.

Commission, E. (2010). Of mice and men – are mice relevant models for human disease? `http://ec.europa.eu/research/health/pdf/summary-report-25082010_en.pdf`. Online, accessed 2015-02-10.

Davidsson, J., Angeria, M., and Risling, M. (2015). Effect of age on amount and distribution of diffuse axonal injury after rotational trauma. Submitted to Frontiers of Neurology.

Farquharson, S., Tournier, J.-D., Calamante, F., Fabinyi, G., Schneider-Kolsky, M., Jackson, G. D., and Connelly, A. (2013). White matter fiber tractography: why we need to move beyond dti: Clinical article. *Journal of neurosurgery*, 118(6):1367–1377.

Hagmann, P., Jonasson, L., Maeder, P., Thiran, J.-P., Wedeen, V. J., and Meuli, R. (2006). Understanding diffusion mr imaging techniques: From scalar diffusion-weighted imaging to diffusion tensor imaging and beyond. *Radiographics*, 26(1):S205–S223.

Hulkower, M., Poliak, D., Rosenbaum, S., Zimmerman, M., and Lipton, M. (2013). A decade of dti in traumatic brain injury: 10 years and 100 articles later. *American Journal of Neuroradiology*, 34(11):2064–2074.

Jbabdi, S. and Johansen-Berg, H. (2011). Tractography: where do we go from here? *Brain connectivity*, 1(3):169–183.

Jones, D. K. and Leemans, A. (2011). Diffusion tensor imaging. In *Magnetic Resonance Neuroimaging*, pages 127–144. Springer.

Ketcham, R. A. and Carlson, W. D. (2001). Acquisition, optimization and interpretation of x-ray computed tomographic imagery: applications to the geosciences. *Computers & Geosciences*, 27(4):381 – 400.

Kingsley, P. B. (2006). Introduction to diffusion tensor imaging mathematics: Part iii. tensor calculation, noise, simulations, and optimization. *Concepts in Magnetic Resonance Part A*, 28(2):155–179.

Komlosh, M. E., Özarslan, E., Lizak, M. J., Horkayne-Szakaly, I., Freidlin, R. Z., Horkay, F., and Basser, P. J. (2013). Mapping average axon diameters in porcine spinal cord white matter and rat corpus callosum using d-pfg mri. *NeuroImage*, 78:210–216.

Krzanowski, W. (2000). *Principles of multivariate analysis*. Oxford University Press.

Kumar, R., Gupta, R. K., Husain, M., Chaudhry, C., Srivastava, A., Saksena, S., and Rathore, R. K. (2009). Comparative evaluation of corpus callosum dti metrics in acute mild and moderate traumatic brain injury: its correlation with neuropsychometric tests. *Brain Injury*, 23(7-8):675–685.

Lavine, G. (2002). Genome project opens new chapter for mice, humans. `http://search.proquest.com/docview/281188662?accountid=10041`, note = Online, accessed 2015-02-10.

Le Bihan, D., Breton, E., Lallemand, D., Grenier, P., Cabanis, E., and Laval-Jeantet, M. (1986). Mr imaging of intravoxel incoherent motions: application to diffusion and perfusion in neurologic disorders. *Radiology*, 161(2):401–407.

Lee, B. and Newberg, A. (2005). Neuroimaging in traumatic brain imaging. *NeuroRx*, 2(2):372–383.

Manley, G. T. and Maas, A. R. (2013). Traumatic brain injury: An international knowledge-based approach. *JAMA*, 310(5):473–474.

Martin, B. (2009). *Nuclear and particle physics: An introduction*. John Wiley & Sons.

Meythaler, J. M., Peduzzi, J. D., Eleftheriou, E., and Novack, T. A. (2001). Current concepts: Diffuse axonal injury–associated traumatic brain injury. *Archives of Physical Medicine and Rehabilitation*, 82(10):1461 – 1471.

Miller, J. A., Horvath, S., and Geschwind, D. H. (2010). Divergence of human and mouse brain transcriptome highlights alzheimer disease pathways. *Proceedings of the National Academy of Sciences*, 107(28):12698–12703.

Mohammadi, S., Möller, H. E., Kugel, H., Müller, D. K., and Deppe, M. (2010). Correcting eddy current and motion effects by affine whole-brain registrations: Evaluation of three-dimensional distortions and comparison with slicewise correction. *Magnetic Resonance in Medicine*, 64(4):1047–1056.

Mori, S. and Zhang, J. (2006). Principles of diffusion tensor imaging and its applications to basic neuroscience research. *Neuron*, 51(5):527–539.

Møller, M. F. (1993). A scaled conjugate gradient algorithm for fast supervised learning. *Neural Networks*, 6(4):525 – 533.

Oxford University Press (2010). Concise medical dictionary. `http://www.oxfordreference.com/view/10.1093/acref/9780199557141.001.0001/acref-9780199557141`.

Park, H.-J., Kubicki, M., Shenton, M. E., Guimond, A., McCarley, R. W., Maier, S. E., Kikinis, R., Jolesz, F. A., and Westin, C.-F. (2003). Spatial normalization of diffusion tensor mri using multiple channels. *Neuroimage*, 20(4):1995–2009.

Paxinos, G. and Watson, C. (2009). *The rat brain in stereotaxic coordinates / George Paxinos, Charles Watson*. Elsevier/Academic, compact 6th ed. edition. Date revised - 2009-02-01; SuppNotes - Previous ed.: Amsterdam : Elsevier, 2007; Includes bibliographical references (p. xx-xxiv) and index; Last updated - 2010-05-03.

Prince, J. L. and Links, J. M. (2006). *Medical imaging signals and systems*. Pearson Prentice Hall Upper Saddle River, NJ.

Seber, G. (1984). Multivariate distributions. *Multivariate Observations*, pages 17–58.

Seel, N. M. (2012). *Encyclopedia of the Sciences of Learning*. Springer Science & Business Media.

Shaw, N. A. (2002). The neurophysiology of concussion. *Progress in Neurobiology*, 67(4):281 – 344.

Siedler, D. G., Chuah, M. I., Kirkcaldie, M. T., Vickers, J. C., and King, A. (2014). Diffuse axonal injury in brain trauma: insights from alterations in neurofilaments. *Frontiers in Cellular Neuroscience*, 8(429).

Silver, J. M., McAllister, T. W., Yudofsky, S. C., and ebrary (e-book collection) (2011). *Textbook of traumatic brain injury*. American Psychiatric Pub, Washington, DC.

Smith, T. B. (2010). Mri artifacts and correction strategies. *Imaging in Medicine*, 2(4):445–457.

Somasundaram, K. and Kalavathi, P. (2012). Analysis of imaging artifacts in mr brain images. *Orient. J. Comput. Sci. Technol*, 5:135–141.

Tortora, G. J. and Derrickson, B. (2013). *Essentials of anatomy and physiology*. Wiley.

Tournier, J.-D., Yeh, C.-H., Calamante, F., Cho, K.-H., Connelly, A., and Lin, C.-P. (2008). Resolving crossing fibres using constrained spherical deconvolution: Validation using diffusion-weighted imaging phantom data. *NeuroImage*, 42(2):617 – 625.

Vikramkumar, Vijaykumar, B., and Trilochan (2014). Bayes and naive bayes classifier. *CoRR*, abs/1404.0933.

Xiong, Y., Mahmood, A., and Chopp, M. (2013). Animal models of traumatic brain injury. *Nature Reviews Neuroscience*, 14(2):128–142.

Yeh, F.-C., Verstynen, T. D., Wang, Y., Fernández-Miranda, J. C., and Tseng, W.-Y. I. (2013). Deterministic diffusion fiber tracking improved by quantitative anisotropy. *PloS one*, 8(11):e80713.

Zhang, H., Yushkevich, P. A., Alexander, D. C., and Gee, J. C. (2006). Deformable registration of diffusion tensor mr images with explicit orientation optimization. *Medical image analysis*, 10(5):764–785.

Zhang, Y., Cai, J., Shields, L., Liu, N., Xu, X.-M., and Shields, C. (2014). Traumatic brain injury using mouse models. *Translational Stroke Research*, 5(4):454–471.

A

Appendix 1

Figures that follow the same procedure used to create figures in section 4.8.2, i.e. figure 4.23, but for the remaining animals are presented below.

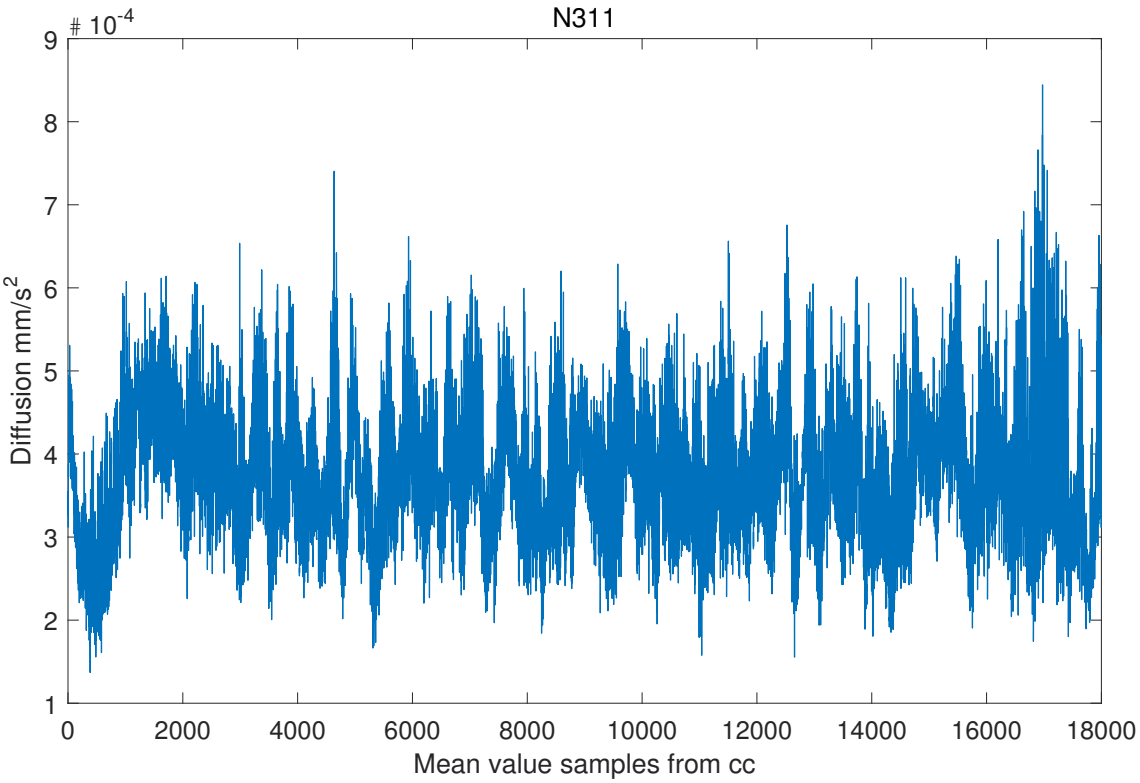

Figure A.1: Mean value for each direction animal N311

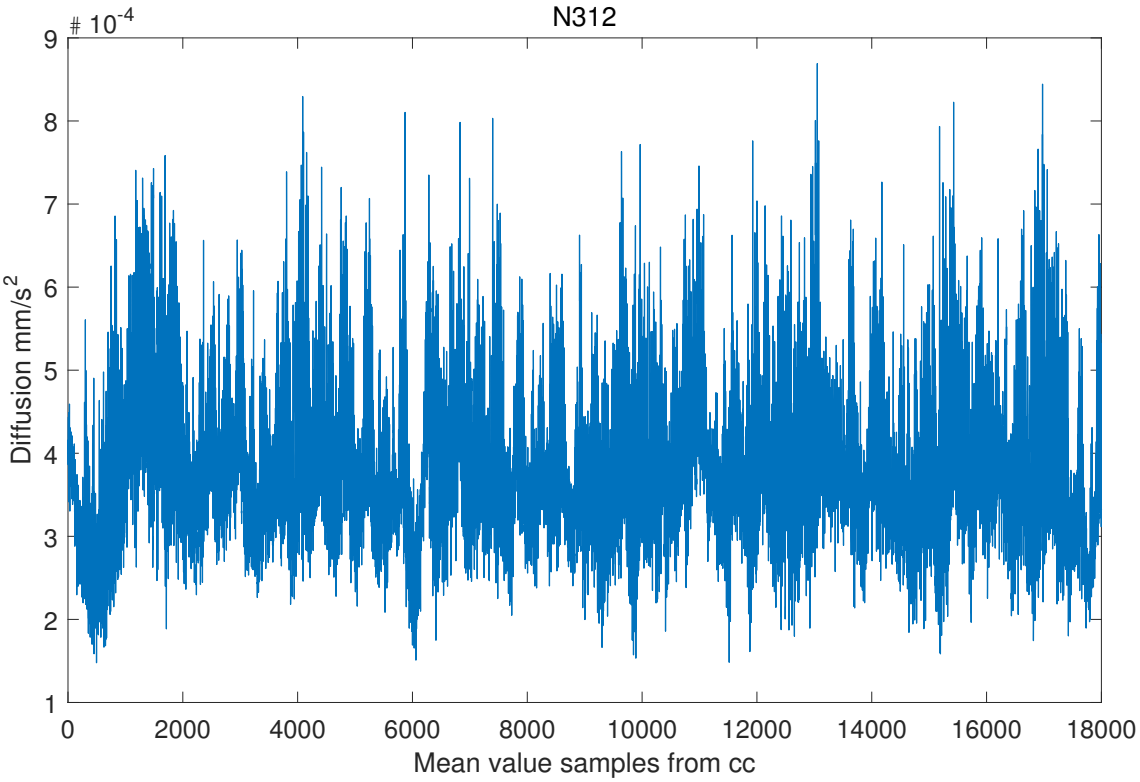

Figure A.2: Mean value for each direction animal N312

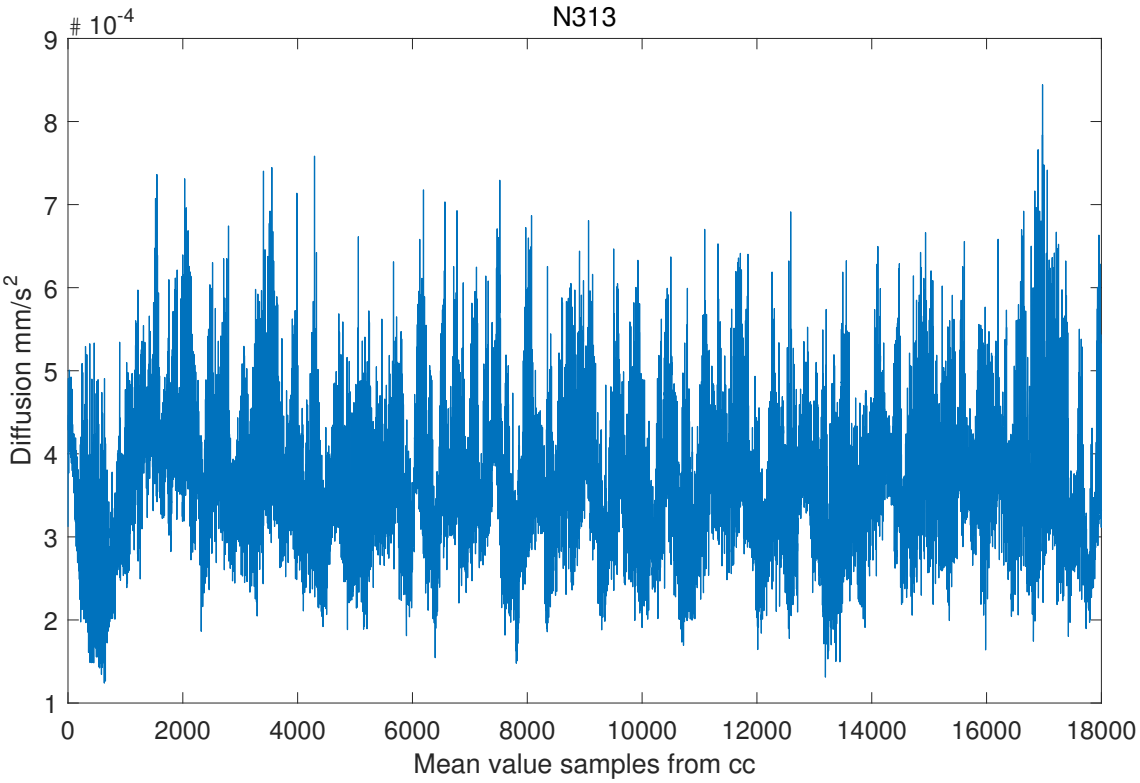

Figure A.3: Mean value for each direction animal N313

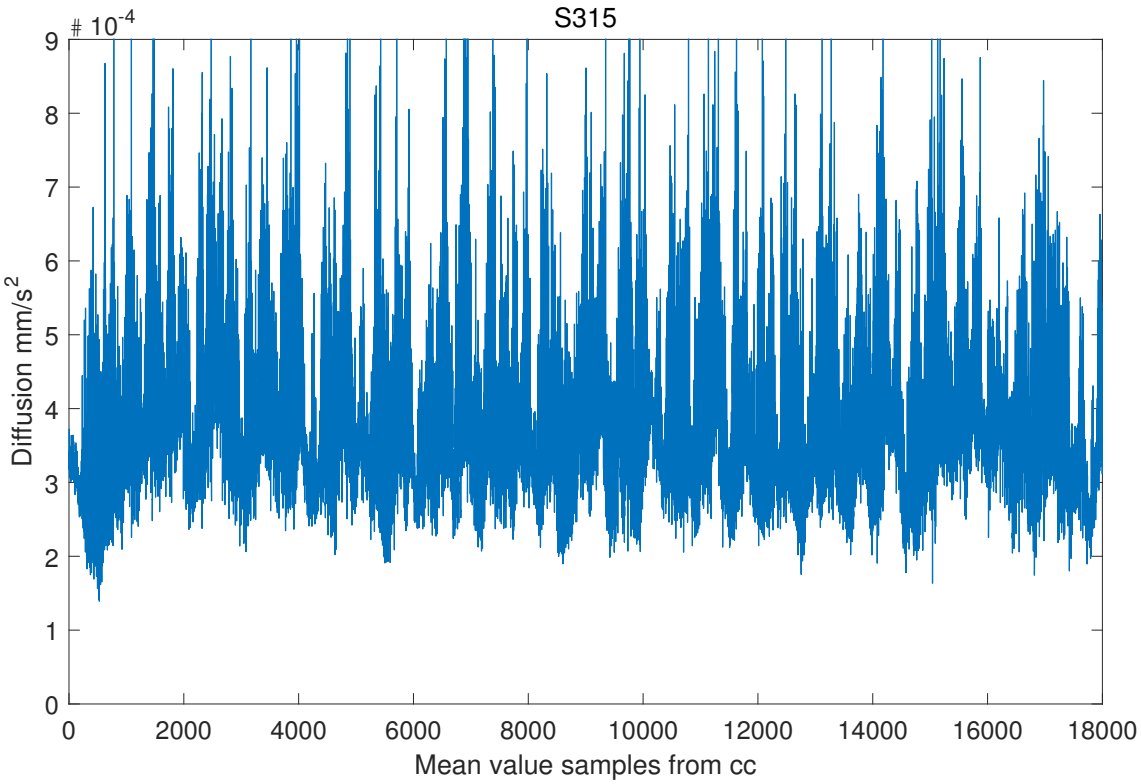

Figure A.4: Mean value for each direction animal S315

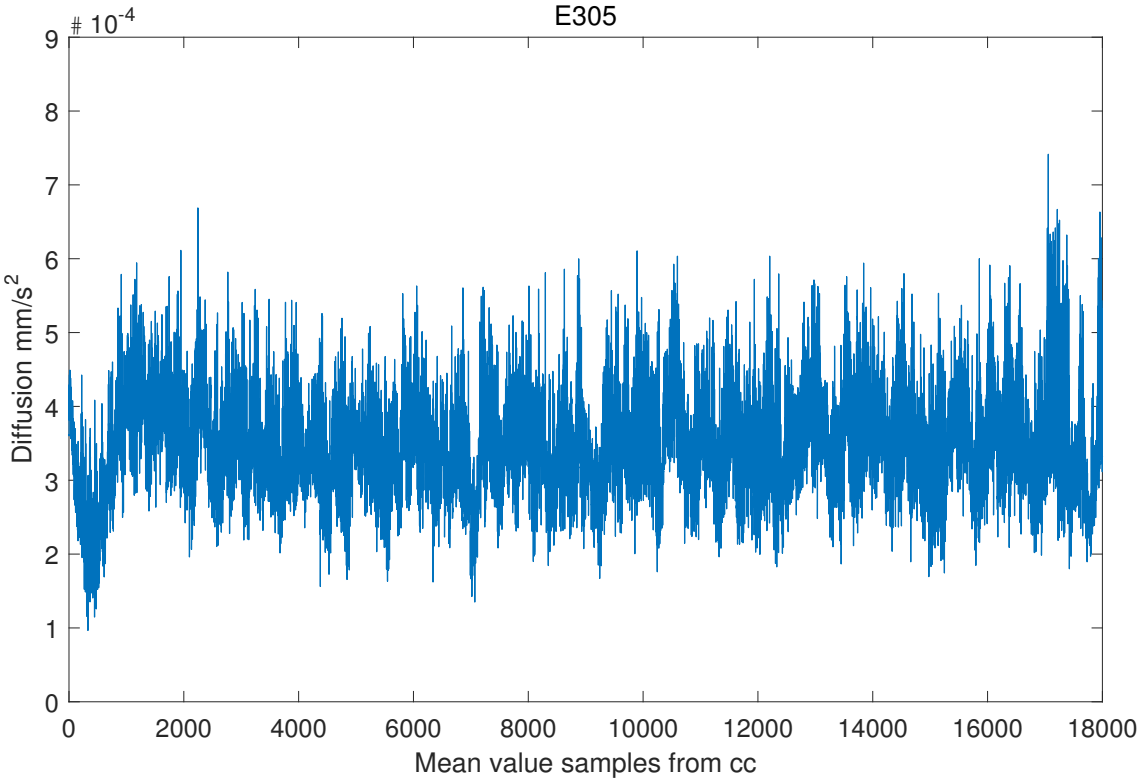

Figure A.5: Mean value for each direction animal E305

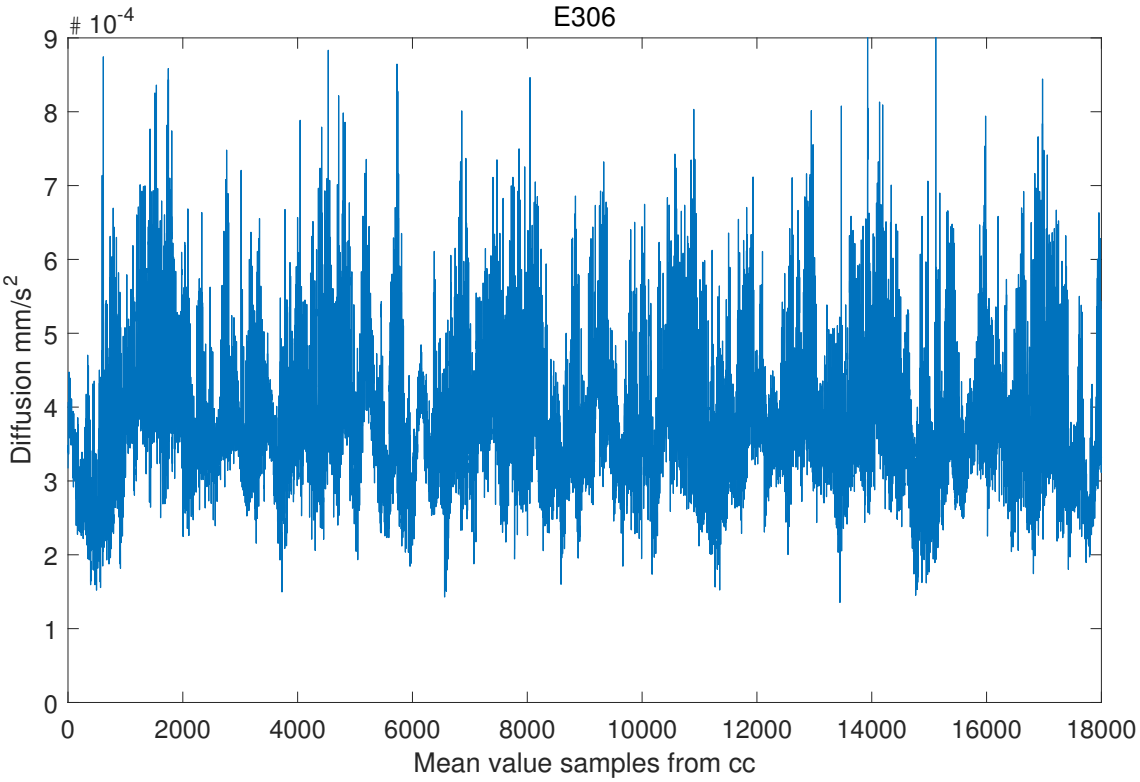

Figure A.6: Mean value for each direction animal E306

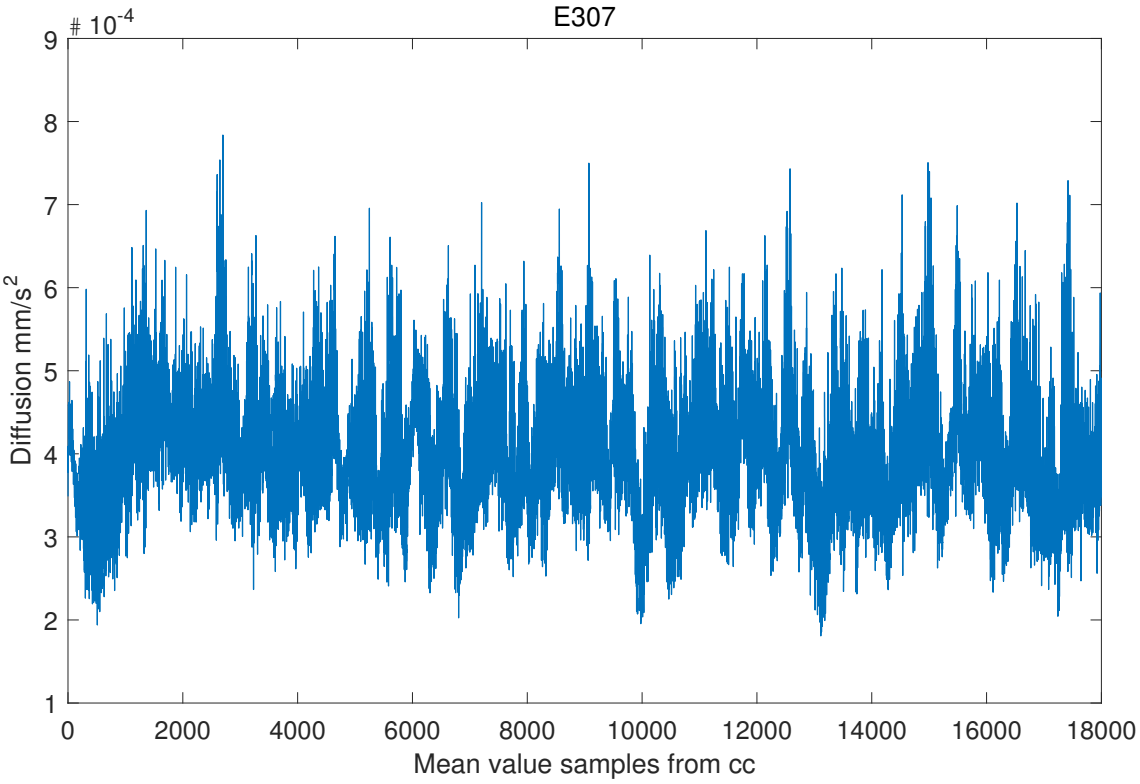

Figure A.7: Mean value for each direction animal E307

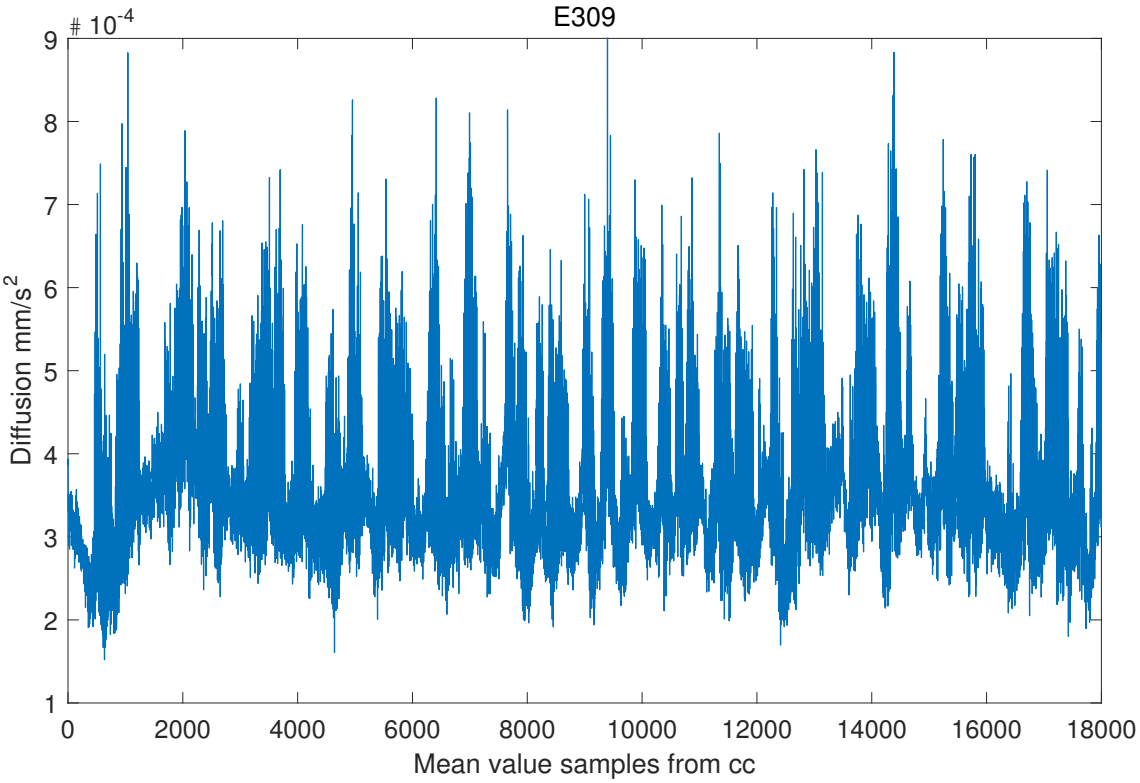

Figure A.8: Mean value for each direction animal E309

Glossary

S_x Diffusion weighted signal.

Affine registration Affine registration is the first step of the spatial normalization used in this thesis, allowing for translation, rotation, scaling and shearing.

Axonal injury Injury to the axons, nerve threads that connect synapses.

b-value Determines sensitivity to diffusion but also the strength, duration of the diffusion gradients.

b0 signal intensity without diffusion weighting.

Biomechanics It refers to the mechanical functions and structures in biological systems.

Bregma The anatomical point on top of the skull where the sagittal- and coronal sutures merge.

Cross-entropy comparing one fixed distribution with another and minimizing the difference between them, in other words finding were they are equal or as close to equal as they can be.

Displacement field The second and final step of the spatial normalization uses displacement fields to align images. The displacement fields in this study are always used on affinely registered images.

Fully aligned Fully aligned, or fully spatially normalized data has been both affinely registered and subjected to displacement fields in order to register the image volumes.

Overfitting It is when datasets is normalized, causing variations between datasets to just be noise or random error and the original distinguishing features are lost.

Pathophysiological changes such as processes or mechanisms inside the body, due to or associated with a disease.

Spin echo Is the reappearance of the NMR signal posterior to the RF pulse which first excite a 90°pulse followed by a 180°refocusing.

Traumatic brain injury An injury where the brain is injured through a blow or penetrative trauma to the skull.

Acronyms

AI Axonal Injuries.

CC Corpus Callosum.

CT Computer Tomography.

DT-MRI Diffusion Tensor Magnetic Resonance Imaging.

DW-MR Diffusion Weighted Magnetic Resonance.

FA Fractional Anisotropy.

MRI Magnetic Resonance Imaging.

ROI Region Of Intrest.

std Standard Deviation.

TBI Traumatic brain injury.

TE Gradient Echo Time.

TR Repetition Time.